BEHAVIOURAL DEFICITS AND MITOCHONDRIAL DAMAGE IN THE LOCUS COERULEUS NEURONS IN A PSEUDO PHOSPHORYLATED HUMAN TAU RODENT MODEL OF ALZHEIMER'S DISEASE

by Jessie Piche, A Thesis submitted

to the School of Graduate Studies in partial fulfillment of the

requirements for the degree of

Master of Science in Medicine (Neurosciences) Faculty of Medicine

Memorial University of Newfoundland

May 2024

St. John’s, Newfoundland and Labrador

Abstract

Early neural abnormality of Alzheimer's disease (AD) involves persistently phosphorylated soluble pre-tangle tau proteins in locus coeruleus (LC) neurons. Cellular toxicity and mitochondrial damage via aggregation of these abnormal tau proteins are thought to induce neurodegeneration early in the progression of AD by compromising metabolic resources in LC neurons. In the current study, behavioural and cognitive functions, along with mitochondrial ultrastructure, were analyzed in a human pre-tangle tau rat model. We infused an adeno-associated viral vector carrying a human tau gene pseudo phosphorylated at 14 sites in 5-month-old TH-Cre rats. Behavioural testing, which took place 10 months post-infusion, showed poorer performance in the spatial and odour discrimination tasks in the pseudo-phosphorylated human tau-infused animals. Following behavioural testing, the animals were perfused, and tissue was embedded for transmission electron microscopy (TEM). Mitochondrial ultrastructural damage was assessed in LC neuronal cell bodies. Results demonstrated a significant increase in mitochondrial damage in the pseudo-phosphorylated human tau-infused rats. These results have the potential to significantly advance our understanding of the early involvement of mitochondrial damage in AD which may lead to earlier detection and potentially, novel therapies for this devastating disease.

General Summary

The Public Health Agency of Canada predicts that the number of individuals living with dementia will rise from 57 million to 83 million in the next decade and to 152 million people by 2050. Alzheimer's Disease (AD) is the most common form of dementia and contributes to the majority of dementia cases. A key component of the development of AD is a protein called tau. Abnormal tau proteins accumulate over decades to form neurofibrillary tangles (NFTs) in the brain which is a major hallmark of AD. These NFTs increase cellular toxicity and mitochondrial damage and are detectable early in the locus coerulus (LC) which suggests that this area is important for the formation of AD. Due to the typically gradual development of AD, there is time to intervene to either slow or stop this disease from developing. This study was conducted to look at how mitochondria in the LC are affected in a pretangle tau animal model. We used a rat model of pre-clinical AD and tested their learning and memory abilities, as well as analyzed their mitochondria through transmission electron microscopy (TEM). We found learning/memory behavioural task impairments were significantly increased in the pretangle tau model as well as increased mitochondrial ultrastructure damage. In sum, these results suggest a promising new target structure (LC) and mechanism (mitochondrial dysfunction) in the effort to slow and hopefully eliminate AD.

Acknowledgments

I would like to express my appreciation to my co-supervisors, Dr. Qi Yuan, and Dr. Andrew Weeks as well as my supervisory committee members, Dr. Xihua Chen, for their incredible support, guidance, teachings, and feedback throughout this project. It has been an honour to work with these individuals.

I would also like to thank my funding sources, without which this project could not have happened. The Memorial University of Newfoundland, which granted me a graduate fellowship, and the Faculty of Medicine Dean's Fellowship, which partially funded this project in adjunction through my supervisor, which was granted to me for this work.

Special thanks to Tonye Omoluabi and Abeni Flynn, whose contributions to this project were significant and made this whole work possible.

I would also like to acknowledge my other lab mates from Memorial University, Ruhuf Abu Labded, Brandon Hannam, Sarah Torraville, Tayebeh Sepahvand, Cassandra Flynn, Zia Hasan, Chelsea Crossley, and Tian Qin. As well as the undergraduate students from Nipissing Univeristy, Carli Hemsworth, Gabrielle Beaulne and lastly, Amy Stillar our laboratory technician. All of these people have helped in the completion of this project and provided me with support and friendship over the past few years. A big thank you should also go to the administrative staff in the Division of BioMedical Sciences and the Faculty of Medicine at Memorial University.

Finally, I'd like to acknowledge my family and friends for their never-ending support while I have pursued this project, these people have been by my side through the most difficult of times, and have provided me with endless happiness, laughs and comfort.

Contributions

I would like to take a moment to give extra thanks to Tonye Omoluabi who performed all the rodent surgeries and who mentored me through all of the behavioural tasks. I would also like to give an extra acknowledgment to Dr. Andrew Weeks and Abeni Flynn who dissected the locus coeruleus for my project. Special thanks to Carli Hemsworth, Gabrielle Beaulne and again Abeni Flynn who assisted me with the work on the transmission electron microscope and the analysis. Without all these individuals this project would not have been successful.

Table of Contents

List of Figures

List of Abbreviations

AAV	Adeno-associated viruses
AC3	Cell apoptosis marker
AD	Alzheimer's disease
ANOVA	Analysis of 16 Variance
APP	Amyloid precursor protein
ATP	Adenosine triphosphate
AT8	Tau-specific monoclonal antibody
DIO	Double-floxed inverted open
EPM	Elevated plus maze
FRT	Food retrieval task
GFP	Control virus
htau	Wild-type human tau virus
htauE14	Pseudo-phosphorylated human tau virus
LC	Locus coeruleus
LTCC	L-type calcium channels
MAPs	Microtubule-associated proteins

MBT	Marble burying test
MRI	Magnetic resonance imaging
mtDNA	Mitochondria deoxyribonucleic acid
NFT	Neurofibrillary tangles
NADH	nicotinamide adenine dinucleotide +hydrogen
NA	Noradrenaline
ODAD	Odour detection and discrimination
OFM	Open field maze
PET	Positron emission tomography
ROS	Reactive oxygen species
SLR	Spontaneous location recall
SOD	Simple odour discrimination
SPT	Sucrose preference test
TH	Tyrosine hydroxylase
TH-CRE	Tyrosine hydroxylase-CRE
TEM	Transmission electron microscopy
4G8	Anti-amyloid-beta monoclonal antibody

List of Appendices

1.0 Introduction

1.1 Overview

Alzheimer's disease (AD) is the most common type of dementia. It is morphological hallmarks are extracellular amyloid plaques and intraneuronal aggregates of tau proteins (Jellinger 2020). Additionally, studies show that mitochondrial dysfunction and oxidative stress play an important role in the early pathology of AD (Moreira et al., 2010). The progression from abnormal phosphorylation of tau to symptomatic and clinical AD occurs over a long period. The present study examines the potential presence of mitochondria damage and dysfunction, as factors that may influence AD development and progression in a pre-tangle rat model.

1.2 Alzheimer's Disease

Alzheimer's disease is an irreversible, neurodegenerative disorder with increasing incidence rates around the world, and is recognized as a global public health priority by the World Health Organization (Lane et al., 2018). The onset of AD is gradual and can span over decades before behaviour/cognitive symptoms become present. The behavioural and cognitive impacts worsen with progression and eventually will take over the life of the person affected. Traditionally, *pre-mortem* diagnoses were not absolute, but further advancements in biomarker identification have led to more confident diagnoses of AD in living patients(Ji et al., 2022). Symptoms of AD can include deficits in cognition and behaviours like memory, learning, language, and recognition (Ji et al., 2022). These deficits typically worsen as one age and the disease progresses. Post-mortem examinations and imaging techniques such as magnetic resonance imaging (MRI), and positron emission tomography (PET) are used to identify the prevalence of both amyloid-beta and Tau proteins in the brain (Jack et al., 2010). These imaging techniques show morphological

abnormalities in the central nervous system, such as expanded ventricles, decreased white matter, brain atrophy as well as increased presence of tau proteins and amyloid-beta (Jack et al., 2010). Neurodegeneration is observed across the brain but is typically more pronounced in areas like the entorhinal cortex, hippocampus, limbic structures, and the locus coeruleus, also known as the LC (López-Cuenca, 2022; Braak et al., 2011).

1.2.1 Hallmarks of Alzheimer's Disease

The two major neurological hallmarks of AD are amyloid-beta plaques and NFTs (Jellinger 2020). Amyloid plaques are extracellular meaning they form within the brain between neurons and they are accumulations of abnormally folded amyloid-beta proteins that limit communication and eventually cause neuronal death (Narayan et al., 2012). NFTs are intracellular meaning they form within the neuron, they are aggregates of hyperphosphorylated tau proteins that cause limitations to intracellular transportation and then result in neuronal death (Serrano-Pozo et al., 2011).

1.2.2 Beta Amyloid Pathology

The amyloid hypothesis, suggests that the accumulation of pathological forms of amyloid-beta is produced by the cleavage of the amyloid precursor protein (APP) (De Strooper et al., 1998). This is completed by beta-secretase to form a C-terminal APP fragment followed by gamma-secretase to form and release amyloid beta into the extracellular space in the brain (De Strooper et al.,1998; Vassar et al., 1999). The progression of AD is driven by an imbalance between amyloid-beta production and amyloid-beta clearance (Vassar et al., 1999). Amyloid deposition does not always follow a stereotypical pattern of progression but typically develops in the isocortex, and only latterly affects subcortical structures (Serrano-Pozo et al., 2011). Unlike NFTs, amyloid plaques involve the entorhinal cortex and hippocampal formations to a lesser extent. (Serrano-Pozo et al., 2011).

Braak and colleagues (1997) examined over 2,600 brains post-mortem, and it was determined that beta-amyloid protein deposits typically appear first in cortical layers III and V, with non-distinct boundaries. These deposits transform into distinct globular plaques. Layers containing myelinated neurons tend to have fewer deposits, while layers with less myelin have denser amyloid deposits (Braak & Braak, 1997).

The initial deposits are found in the perirhinal and entorhinal cortices, occurring as early as young adulthood (Braak & Braak, 1997). These plaque deposits then increase in number and spread to nearby areas, such as the neocortex and hippocampal formation. Spread continues gradually until all areas of the cortex are affected, including myelinated areas, in much later stages (Braak & Braak, 1997).

While amyloid plaques were originally thought to be critical to the development of AD, it is now thought that soluble amyloid-beta oligomers may be the most pathological forms (Narayan et al., 2012). Oligomers purified from AD brains and applied to neurons in vitro inhibit long-term potentiation, cause synaptic dysfunction, damage dendritic spines and cause neuronal death (Shankar et al., 2008). With this outlook, plaques may act as a 'reservoir' from which amyloid oligomers diffuse, or may even act as a protective mechanism sequestering toxic amyloid-beta proteins (Narayan et al., 2012).

The accumulation of amyloid-beta is a biomarker of AD. However, the fact that a significant proportion of elderly individuals die with evidence of significant amyloid-beta deposition without any cognitive symptoms proves that it is not a sufficient sole biomarker for AD dementia. In a study conducted by Esparaza and colleagues (2018) amyloid-beta oligomers and plaque pathology were detected in aqueous cortical lysates from patients with dementia of the Alzheimer type as well as in patients without dementia. Amyloid-beta oligomer concentrations in

patients with dementia were tightly correlated with beta-amyloid plaques. This relationship was seventy-five percent weaker in those from patients without dementia, despite equivalent amyloid-beta plaque pathology there were much higher concentrations of soluble amyloid-beta oligomers. The absolute oligomer: plaque ratio may be lower in patients with asymptomatic amyloidosis than in patients with AD dementia, supporting the concept that plaques may act as a protective reservoir (Esparaza et al., 2018).

1.2.3 Tau Pathology

Tau is a vital part of the process that leads to AD, as evidenced by the requirement for both beta-amyloid and tau pathology for a diagnosis of AD and the close association between neurodegeneration and tau load (Tsuboi et al., 2005). A study examining brains from 1 to 100 years old demonstrated that abnormal tau preceded amyloid deposits; with tau pathology beginning as early as the first decade of life, and amyloid pathology primarily occurring from at least the fourth decade of life (Braak et al., 2011).

Tau plays a key role in the cytoskeleton by binding to and stabilizing microtubules that maintain cellular morphology and intracellular transport (Szabo et al., 2020). Tau is a member of the microtubule-associated proteins (MAPs) family, and it was discovered in the 1970s as a protein that copurifies with tubulin (Weingarten et al., 1975). Tau plays a central role in the assembly disassembly and spatial organization of microtubules. Tau and other MAPs that bind to microtubules are tightly regulated by several factors to ensure the appropriate dynamics of the system (Mandelkow et al., 1995). Tau is found as six molecular isoforms in the human brain, tau consisting of four related polypeptides with apparent molecular weights of 50,000 to 68,000. (Goedert et al., 1989). The carboxyl-terminal of these isoforms contains half a region of three or

four tandem repeats of 31 or 32 amino acids, each displaying a characteristic that represents the tubulin-binding domain (Himmler et al., 1989).

Tau is a phosphoprotein and in an adult brain, it is phosphorylated at two or three sites on all six isoforms (Goedert 1993). Tau contains a particularly high content of serine and threonine, many of which are phosphorylated under physiological conditions (Götz et al., 2007). Under pathological conditions, tau becomes hyperphosphorylated, which means a higher degree of phosphorylation at these physiological sites. Phosphorylation decreases the binding affinity of tau to microtubules. This then increases the pool of soluble tau and is thought to trigger the disassembly of microtubules (Götz et al., 2007). The largest human brain tau isoform contains 17 serine/threonine-proline sites, a cluster of serine/threonine-proline sites is present in a proline-rich region of the protein, and a smaller cluster at the carboxy-terminal end (Goedert 1993). Several phosphorylation sites have been identified through the use of mass spectrometry and phosphorylation-dependent antibodies (Goedert 1993). Persistently phosphorylated tau can aggregate into NFTs, a hallmark biomarker of AD (Szabo et al., 2020).

While tau dysfunction and toxicity have been linked to the formation of soluble oligomeric structures, these early intermediates are difficult to study in complex samples such as the human brain (Ercan-Herbst et al., 2019). While more than 70 phosphorylation sites have been detected previously on NFT tau, studies of oligomeric and detergent-soluble tau in human brains during the early stages of AD are lacking. The study conducted by Ercan-Herbst, and colleagues (2019) found that soluble tau multimers are strongly increased at Braak stages III–IV in all brain regions under investigation, including the temporal cortex, which does not contain NFTs or misfolded oligomers at this stage of pathology. It was additionally identified that five phosphorylation sites are specifically and consistently increased across the entorhinal cortex, hippocampus and temporal

cortex. Three of these sites correlate with tau multimerization in all three brain regions but do not overlap with the epitopes of phospho-sensitive antibodies commonly used for the immunohistochemical detection of NFTs. These results suggest that soluble multimers are characterized by a small set of specific phosphorylation events that differ from those dominating in mature NFTs. These findings shed light on early post-translational modification changes of tau during AD pathogenesis in human brains (Ercan-Herbst et al., 2019).

Tau is probably the most studied MAP because of its implication in a group of neurodegenerative diseases called tauopathies, associated with Tau aggregation into intraneuronal deposits (Barbier et al., 2019). Tauopathies occur when the deviant tau begins to accumulate in the cell, resulting in a propagation of protein misfolding (Szabo et al., 2020).

Bierer and colleagues (1995) studied the measures of NFTs and plaques in the hippocampus and neocortex of seventy cases of clinically and neuropathologically confirmed AD. Among these scores, only NFTs in the neocortical regions showed a significant association with the Clinical Dementia Rating Scale. NFT densities in the superior temporal cortex were most strongly correlated with dementia severity, followed by those in the inferior parietal and mid-frontal cortex. No such correlations were apparent for the amygdala, hippocampus, or entorhinal cortex. Medial temporal lobe structures displayed high NFT scores, even in cases of mild dementia. Meanwhile, plaque density correlated with age at death, but there is no correlation between plaque counts and dementia severity nor did they correlate significantly with the Clinical Dementia Rating Scale score in any region. This data supports the notion that neocortical neuronal degeneration, as indicated by NFT formation, is a critical determinant of the clinical progression of AD and suggests that medial temporal lobe structures may represent the initial site of NFT formation (Bierer et al., 1995).

In a different study, Braak and colleagues (2011) used a tau-specific monoclonal antibody (AT8) and Gallyas silver staining for abnormal tau, anti-amyloid-beta monoclonal antibody (4G8) and Campbell-Switzer staining for the detection of hyperphosphorylated tau and amyloid-beta in the brains of 2332 people. Pretangle stages a-c were observed as early as the first decade and were present in the majority of samples by the second decade. During these stages, aberrant pretangle tau formed in the transentorhinal region without cortical projections and in the LC. Then, as early as the second decade, pretangle stages 1a and 1b were observed and were found in the majority of samples by the fourth decade. During these stages, in addition to the subcortical lesions from stages a-c, some cortical lesions were also visible in the temporal lobe. Neurofibrillary stages I–VI were assigned to the samples once the aberrant tau turned insoluble and started to form NFTs. The transentorhinal region, the entorhinal region, the hippocampal formation, the cortical areas starting in the temporal lobe, the frontal and insular areas, the prefrontal cortex and association cortices, and lastly the premotor and primary motor areas were where the NFTs were first observed for these stages. In the third and fourth decades, pretangle stages 1a and 1b, amyloid-beta deposits started to form. The eighth and ninth decades are when the more recent phases V and VI gained prominence. Given the onset of aberrant tau, this would imply a significant function for the LC in the development of AD (Braak et al., 2011).

1.2.3.1 Locus Coeruleus

AD is significantly associated with selective degradation of subcortical projection neuronal cells, including the noradrenergic neurons of the LC (Patel et al., 2012; Grudzien et al., 2006). Neuronal Tau aggregates may appear early in life, in the absence of clinical symptoms (Giorgi et al., 2017). This occurs in the brainstem reticular formation and mostly within the LC which is consistently affected during AD. The isodendritic nature of LC neurons allows their axons to spread

noradrenaline (NA) throughout the whole forebrain (Giorgi et al., 2017). The LC contains a tube-like-shaped group of NA neurons located in the rostral part of the pons. It is a small nucleus located bilaterally in the brainstem and is found ventral to the fourth ventricle (Poe et al., 2020).

The LC releases NA in the cortical and hippocampal regions of the brain (Counts & Mufson, 2010). NA signalling is fundamental for a range of behavioural responses such as memory storage/retrieval, selective attention, arousal, mood, vigilance functions, sleepwaking cycle, alertness, and synaptic plasticity (Giorgi et al., 2017; Weinshenker 2008). Counts and Mufson, (2010) identified that NA protects target neurons from amyloid toxicity by preventing amyloid beta-induced increases in oxidative stress, mitochondrial dysfunction, and the activation of apoptotic pathways. These findings support their hypothesis that NA confers neuroprotection. Thereby, a potential consequence of LC neurodegeneration may be the reduction in signalling in LC projection sites in AD. This sheds more insight into the mechanistic consequences of LC degeneration during the pathogenesis of AD (Counts & Mufson, 2010).

Results from a study conducted by Grudzien and colleagues (2006) showed that the LC develops fully formed NFTs and their precursors in the course of normal aging but that these abnormalities become significantly more prominent in the early stages of AD. Evidence has shown that even early stages of neurofibrillary degeneration can interfere with normal cellular functioning (Hatanpää et al., 1996). Such changes can have particularly far-reaching consequences when they involve the LC. The presence of fully formed NFT and their precursors in the LC even at very early Braak and Braak stages also establishes that the LC is one of the few regions in the brain with a very high susceptibility to neurofibrillary degeneration (Grudzien et al., 2006). Only neurons located within the boundaries of the LC invariably depicted NFT or AT8 (a tau-specific monoclonal antibody that is a commonly used marker of neuropathology because it recognizes

abnormally phosphorylated tau) immunoreactivity. The numerous surrounding nuclei were all uniformly free of such pathology. This study conclusively demonstrated that LC tauopathy is a component early stages of AD (Grudzien et al., 2006).

Another study conducted by Wilson and colleagues (2013) had 165 participants from the Rush Memory and Aging Project. After death, the brains were examined and provided estimates of the density of aminergic neurons in the locus coeruleus as well as in other nuclei and measures of neuronal neurofibrillary tangles from these areas. The results indicated LC neuronal density was related to cognitive decline. The density of noradrenergic neurons in the LC demonstrated to be a structural component of neural reserve (Wilson et al., 2013).

This brain region is a highly connected area having tracts to multiple brain structures, notably the entorhinal cortex around the hippocampus – a structure involved in memory (Braak et al. 2011). Pathologies of AD occur in the LC early in disease progression, thus making it an ideal location to experimentally explore neurodegeneration and intracellular deviations induced early in AD. Understanding these changes may allow for early interventions before disease progression before irreversible damage has occurred.

1.2.3.2 Animal Model of Pretangle Tau

An animal model of AD was established by Gosh and colleagues (2019) based on the findings of Braak's research on the pretangle stages (Braak et al., 2011). This was achieved by infusing a genetic construct of pseudo-phosphorylated human tau (htauE14) in a viral vector bilaterally into the LC of tyrosine hydroxylase-CRE (TH-CRE) rats. The study concluded that AD animals had lower performances on a difficult olfactory discrimination task 7-8 months post-infusion than controls, however, not 4 months post-infusion when the vector is infused at a young age (2-3 months old). This was accompanied by reduced NA fibre density seen in the piriform cortex. Additionally, AD animals were unable to complete a simple olfactory discrimination task at 5-6

months post-infusion, when infused at an older age (14-16 months old). This was also accompanied by a loss of LC cells, and a more potent spread of tau (Ghosh et al., 2019). While htauE14 affects synaptic function similarly to biologically phosphorylated mutant tau associated with frontotemporal dementia (Hoover et al., 2010), mutant tau related to frontotemporal dementia is not typically found in the LC (Yang and Schmitt, 2001), making it an inadequate model for pretangle AD tau. Other efforts to replicate pretangle tau in the LC have been unsuccessful. In mice, the introduction of AD tau fibrils near the LC resulted in tau hyperphosphorylation in LC neurons, but the spread of this hyperphosphorylated tau did not mirror the patterns observed in humans (Iba et al., 2015). The htauE14 model allows for targeted expression of a continuously phosphorylated form of human tau specifically in the LC neurons (Ghosh et al., 2019). The impact of htauE14 is significantly influenced by age, with more pronounced effects observed in older rats where htauE14 expression leads to more severe pathophysiological outcomes (Ghosh et al., 2019). This is the model that was used in this study. It was generated to provide an animal AD model that can be used to better understand pretangle tau pathology.

1.3 Mitochondria in Aging

Mitochondria are found in nearly all eukaryotic cells (Osellame et al., 2012). They are membrane-bound organelles, and their morphology is highly important for their function. They are essential to the preservation of life and the guardians of cell death because they coordinate the synthesis of cellular energy known as adenosine triphosphate (ATP). Their remaining genome is represented by mitochondria deoxyribonucleic acid (mtDNA), which codes for many proteins necessary for the respiratory chain's operation (Anderson et al., 1981). The aqueous area between the inner and outer maintains space is called the intermembrane space (Friedman & Nunnari 2014). The inner

membrane forms several folds, this is called cristae which extends into the interior of the organelle which is called the matrix space (Friedman & Nunnari 2014). Numerous essential cellular activities, including calcium signalling, cell growth and differentiation, cell cycle regulation, and cell death, are facilitated by mitochondria (Duchen 2000; Osellame et al., 2012; Susin et al., 1999). The importance of fission and fusion homeostasis has been highlighted by several disease states, an imbalance in fission and fusion events often leads to a distinct shift in the morphology and viability of the organelle (Palmer et al., 2011). Mitochondrial dysfunction is implicated in metabolic and age-related disorders, neurodegenerative diseases and ischemic injury in the heart and brain (Osellame et al., 2012).

Aging impairs mitophagy; which is the removal of stressed mitochondria (Jang et al., 2018). The age-dependent decline in mitophagy might provide the mechanism to explain the known interrelationship between increased reactive oxygen species (ROS), decreased bioenergetic capacity, and age-dependent functional decline (Harman 1972; Jang et al., 2018). Damaged mitochondria can signal back to the nucleus to orchestrate a nuclear transcriptional response that reduces mitochondrial stress and thereby prevents subsequent damage (Jang et al., 2018). These retrograde signalling pathways are increasingly being seen as critical for maintaining functional capacity in aging tissues.

Age-related changes in mitochondria are associated with a decline in mitochondrial function (Chistiakov et al., 2014). With age, mitochondrial DNA volume, integrity and functionality decrease due to the accumulation of mutations and oxidative damage induced by reactive oxygen species (ROS) (Harman 1972). In aged subjects, mitochondria are characterized by impaired function such as lowered oxidative capacity, reduced oxidative phosphorylation, decreased ATP production, a significant increase in ROS generation, and diminished antioxidant

defence (Chistiakov et al., 2014). Mitochondrial biogenesis declines with age due to alterations in mitochondrial dynamics and inhibition of mitophagy (Cortopassi & Arnheim 1990). Age-dependent abnormalities in mitochondrial quality control further weaken and impair mitochondrial function (Chistiakov et al., 2014). In aged tissues, enhanced mitochondria-mediated apoptosis contributes to an increase in the percentage of apoptotic cells (Marzetti & Leeuwenburgh 2006).

Mitochondria have been traditionally viewed as simple, autonomous energetic factories whose waste product fueled the aging process. As the knowledge of this organelle has expanded, so too have the connections between mitochondrial function, aging and neurodegenerative diseases.

1.4 Role of mitochondria in AD

1.4.1 Mitochondria and Tau

Microtubules are the fundamental organelle for fast axonal transport, which is essential for the renewal of axons and membranes in the nerve terminal. Defective microtubule assembly and stabilization in neurons could lead to impaired axonal transport and abnormal synaptic transmission (Shahpasand et al., 2012). A study by Shahpasand and colleagues (2012) discovered that the overexpression of tau increases the pausing frequency of mitochondria movement by sixteen percent in neurons. In addition, overexpression of tau reduces the anterograde movement of mitochondria, suggesting that tau itself inhibits mitochondrial transport independent of its posttranscriptional modification state (Shahpasand et al., 2012; Vossel et al., 2010).

Phosphorylated tau has been shown to inhibit anterograde transport, leading to the possibility of mitochondrial cluttering in the soma and a lack of mitochondrial numbers at synapses (Ittner et al., 2008). Phosphorylated tau inhibits complex I in the electron transport chain and increases the production of ROS (Schulz et al., 2012). Mitophagy may be inhibited by the presence

of abnormal tau thus resulting in the accumulation of damaged mitochondria in the neuron (Schulz et al., 2012). Additionally, in a study conducted by Li and colleagues (2016) inducing human wild-type full-length tau in rodents increased mitochondrial fusion. Overall, overexpression of the tau protein negatively impacts mitochondrial functioning by inhibiting electron transport chain complexes, antioxidants, and repair processes in the mitochondrion (Li et al., 2016).

Abnormal tau protein has been found to cause mitochondrial dysfunction that leads to neurodegeneration (Szabo et al., 2020). Importantly, the exact mechanisms underlying this effect are not fully understood. One prediction through which tau may induce mitochondrial dysfunction is through interactions with calcium channels in the cell membrane (Ryan et al., 2020).

1.4.2 Mitochondria and Calcium

Dysregulation of mitochondrial calcium homeostasis has long been implicated in AD pathology (Walker & Moraes 2022). Cellular calcium concentration must be highly regulated for proper cellular functions. In neurons, calcium plays different roles depending on spatial localization and neuronal type (Walker & Moraes 2022). Regulation of calcium is important for both synaptic transmission and vesicle recycling (Cid-Castro et al., 2018). Calcium overload, as induced by prolonged stimulation of glutamate receptors, consequently, results in cell death, a process termed excitotoxicity (Celsi, et al., 2009). In AD, impaired homeostasis may be due to increased mitochondria-associated endoplasmic reticulum membrane contact or altered expression of mitochondrial ion exchangers (Jadiya et al., 2019). An increase in mitochondrial calcium can stimulate ROS production and decrease ATP production, both of which can activate retrograde signalling pathways, as well as provoke permeability transition pore opening and induce apoptosis (Jadiya et al., 2019). Mitochondria can uptake calcium through the outer membrane to bring calcium into the matrix (Walker & Moraes 2022). Several dehydrogenases in the matrix are

sensitive to calcium, therefore influencing ATP synthesis via nicotinamide adenine dinucleotide plus hydrogen (NADH) availability and electron flow (Rizzuto et al., 2012). High concentrations of calcium can stimulate the opening of the permeability transition pore and induce apoptosis or necrosis, while low concentrations may stimulate pro-survival autophagy due to decreased ATP concentrations (Rizzuto et al., 2012). Ultimately, in cells experiencing mitochondrial dysfunction, increased cytoplasmic calcium leads to alteration in the activity of cell proliferation transcription factors and even expression of anti-apoptotic markers (Amuthan et al., 2002; Arnould 2002; Biswas 1999).

Signals originating from the mitochondria, including calcium, ROS, and ATP, often stimulate pathways, leading to transcriptional changes in the nucleus. Nuclear responses can involve upregulating cell proliferation and anti-apoptotic factors, as well as proteins involved in mitogenesis (Walker & Moraes 2022). The main pathway for calcium entry is via L-type calcium channels (LTCC), which can modulate calcium influx to couple neuronal excitation states to neuronal gene expression (Moore & Murphy, 2020). Age-related deficiencies like memory loss and learning, as well as illnesses like Alzheimer's, are influenced by this dysregulation (Moore & Murphy, 2020). According to Hotka and colleagues (2020), LTCC-mediated calcium influx affects mitochondrial function, which is essential for controlling cell viability. In neurologic disorders, mitochondrial calcium excess causes cell apoptosis (Hotka et al., 2020). Overall, mitochondrial dysfunction is common in AD and likely plays a role in disease progression (Walker & Moraes 2022).

1.5 Hypothesis

LC fiber degeneration with pretangle tau incubation has been observed in a previous study (Ghosh et al., 2019). Looking at the relationship between phosphorylated tau and mitochondria it is hypothesized that the impairment of LC neuronal health by pre-tangle tau is associated with mitochondrial dysfunction in a rat pretangle tau model. The objective of this study is to use TEM to test whether there would be a difference in ultrastructure in the mitochondria of LC cell bodies. It is hypothesized that the rodents with LC neurons depicting the most mitochondria ultrastructure damage will correlate with the rodents that showed decreased learning/memory-making abilities. This in turn would correlate with how rodents modelling symptoms of Alzheimer's may have impaired ability to form memories and are experiencing significant mitochondrial damage within the LC.

2.0 Materials and Methods

2.1 Viral Infusion

2.1.1 Subjects

The total number of subjects for the behaviour portion of this study was twenty-five TH-Cre rats both male and female separated into two cohorts; the first cohort had seventeen animals and the second had eight animals. Twenty-five subjects were analyzed through TEM, only eighteen were accounted for in the final analysis. This was due to inadequate perfusions, limiting the proper use of the TEM. A total of nine cells (three neurons per depth, one thousand micrometres apart to ensure a new neuron was selected, for a total of three depths per brain) per brain were analyzed at the TEM level. Both the right and left hemispheres were analyzed and selected at random. Animals were randomly assigned to one of three groups, two experimental and one control

group. Subjects were housed individually and given unlimited access to dry food pellets and water. They were housed with standard enrichment in standard cages in a reverse twelve-hour light-dark cycle. Behaviour tests occurred throughout their light cycle. All animal housing and experimental procedures were approved by Memorial University of Newfoundland's Institutional Animal Care Committee and followed the Canadian Council on Animal Care guidelines.

2.1.2 Viral Vectors

A virus containing the genetic construct for a wild-type human tau (htau), or with a pseudo-phosphorylated human tau (htauE14) or a control virus (GFP) was infused into rats. Since pseudo-phosphorylated tau has been demonstrated to mimic the effects of persistently phosphorylated tau (Hoover et al., 2010), the htauE14 plasmid was selected. This plasmid was made available on Addgene by Karen Ashe Lab Materials, and it contains approximately eighty percent of the seventeen possible serine/threonine-proline sites pseudo-phosphorylated, which is consistent with sites frequently impacted by abnormal tau linked to AD. The three viral vectors had a green fluorescent protein tag and double-floxed inverted open (DIO) reading frames, which made them Cre-inducible to guarantee cell-specific targeting. This indicates that the construct-containing sequence is inverted in the vector, and tyrosine hydroxylase (TH) positive cells, Cre-recombinase flips the sequence to its proper orientation. The AAV9-rEF1a-DIO-htauE14-EGFP (1.3e13 vg/ml, Source: Vivorek (15-398)) and AAV2/DJ-Ef1a-DIO-EGFP-htau_WT (2.35e13vg/ml, Source: neurophotonics (Laval, 1594)) served as the viral vector for experimental animals (htauE14 and htau, respectively), whereas AAV9-rEF1a-DIO-EGFP (1.5e13 vg/ml, Source: Vivorek (17-087)) served as the control virus.

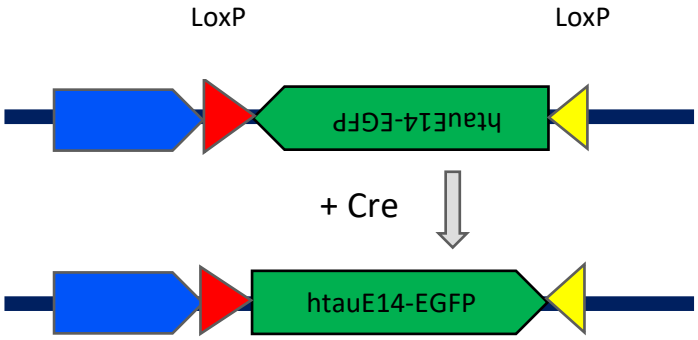

Figure 1. Cre-recombinase mechanism.

2.1.3 Infusion Surgery

Similar to what Ghosh and colleagues (2019) have reported, the rats underwent viral infusion operations between the ages of two and three months. The animals were put in a stereotaxic apparatus with their skulls flat after being anesthetized with three percent isoflurane. To prevent hypothermia, the animals were placed on a heating pad that was covered with a puppy pad. Cling wrap covered the animals and maintained the surrounding heat. Subcutaneous injections of Meloxicam Slow Release (10 mg/ml) were used as an analgesic. Sensorcaine Epinephrine (0.25%, 0.25 ml) was used as a local anesthetic and vasoconstrictor to minimize bleeding along the incision line. Using a microdrill, holes were made 11.6–12.9 mm posterior and 1.3 mm bilaterally to Bregma in the skull. An infusion pump and guide cannula positioned in a parasagittal plane at a twenty-degree angle caudal to the coronal plane were used to complete an infusion of 1µl of the virus combined with 0.4µl of blue fluorescent beads at two sites within LC on each side (a total of four infusion sites). The LC coordinates are 6.3 mm ventral from the brain surface, 12.0-13.7 mm posterior, and 1.2-1.4 mm bilateral to the Bregma. After surgical procedures were completed, they

were kept overnight in a clean cage with a heating pad. A minimum of 10 months was given to the animals to heal after surgery before starting any behavioural tests.

The same model was used in this study as per Ghosh and colleagues (2019). This model has been highly validated with infection rates greater than eighty percent (Ghosh 2019; Omoluabi 2021). When performing a transcardiac perfusion for TEM it excludes the possibility of doing IHC, therefore preventing the ability to check transfection in the LC. However, we are confident that the proper location was targeted.

2.2 Behavioral Experiments

All behavioural tasks were conducted blindly, meaning the groups in which each animal was remained unknown. All tasks were completed in the same order to maintain control for all cohorts. The animals were also always tested in the same order within the cohorts, as well as at similar times for the multiple-day tasks.

2.2.1 Subjects

All subjects GFP (control), htau (experimental) and htauE14 (experimental) in these groups underwent the same behavioural tests.

2.2.2 General Behaviour Experiments

2.2.2.1 Sucrose Preference Test

Water was withheld from the animals for a full day before the sucrose preference test (SPT) commenced. Two identical water bottles were given to each animal; one held ordinary tap water, and the other held a tap water-based 0.1% sucrose solution. Before the bottles were given to the animals, they were all weighed. Twenty-four hours after the SPT started, the bottles were taken out of the cages and weighed. When the bottles were available, the animals could access them as

often as ad libidum. During the test, the ratio of sucrose consumed to total fluid consumed was noted. Anhedonia (inability to feel pleasure) is indicated by a decreased preference for sucrose (Liu et al., 2018).

2.2.2.2. Marble Burying Test

Sixteen identical dark-blue marbles were set up in a 4 x 4 grid on sanitized extra bedding in a clean cage for the Marble Burying Test (MBT). The animals were videotaped while they were in the cage for thirty minutes. It was noted how many marbles were at least seventy-five percent buried in bedding. Increased stress-like symptoms are indicated by a higher number of marbles buried (Archer et al., 1987). The effects of the virus between groups on stress-like symptoms were determined by the number of marbles buried.

2.2.2.3. Elevated Plus Maze

The animals were tested in a five-minute trial on an elevated plus maze (EPM). The EPM arm measures 50 x 10 cm, with a platform in the centre measuring 11 x 11 cm. It is elevated 52 cm above the ground and has a wall height of 38 cm. The trials were captured on camera, and the animals were positioned with their backs to the researcher and toward an open arm. The number of head dips (dipping the head over the edge of the maze from the open arm) and the amount of time in both closed and open arms (when all four paws are within the arm boundary) were noted. Higher levels of stress-like symptoms were correlated with shorter head dips and more time spent in the closed arms (Kraeuter et al., 2019). Time spent in the closed and open arms, as well as the number of head dips, were used as indicators of stress-like symptoms.

2.2.2.4. Open Field Maze

For a ten-minute trial, animals were housed in an open field maze (OFM) measuring 60 x 60 x 50 cm. Throughout the trial, animals were free to roam around the maze, and it was captured by

camera. The ANYMaze software program was used to record the average speed and distance travelled; manual records were made of the amount of time spent freezing and rearing. Reduced maze exploration was a sign of more symptoms similar to stress (Seibenhener & Wooten 2015).

2.2.3 Learning Experiments

2.2.3.1 Spontaneous Location Recall

Bekinschtein and colleagues (2013) state that the spontaneous location recall (SLR) test necessitates a training and testing phase to test memory-making abilities. A soda can with the logo facing toward the centre of the box was positioned against one wall of the OFM apparatus, 30 cm from each corner, for the training phase. With their logos facing the centre of the box, two more identical soda cans were positioned against the opposite wall, 10 cm apart and 10 cm from each corner. After being put inside the box, the animals had ten minutes to freely investigate the cans and the box. During the recall phase, twenty-four hours later an identical soda can to the others was set up in the same spot as the first can from the training phase for the testing phase; this was referred to as the familiar location object. With the logo facing the centre of the box, this new, identical can become the novel location object. It was positioned on the opposite wall, in the centre of where the other two cans from the training phase had been placed. For ten minutes, the animals were free to investigate the box's new configuration. During the training and testing phases, the amount of time spent examining every object was noted. Animals were supposed to have spent about the same amount of time investigating each of the three objects during the training phase. An indication that the animal remembered the training phase occurred when it spent more time investigating the new object location during the testing phase.

2.2.3.2 Odour Detection and Discrimination

The goal of odour detection and discrimination (ODAD) was to test the animals' capacity to recognize and distinguish between similar smells in preparation for olfactometer training. Animals were housed in a sterile mouse cage and given mineral oil three times, followed by odour one (which contained 0.001% heptanol) and odour two (which contained 0.001% heptanol and octanol in a 1:1 ratio in mineral oil) three times each. Filter paper (60 ul) was saturated with odours, which were then presented in tiny, perforated tubes through the openings of the cage for fifty seconds, interspersed with five-minute intervals. When the animals first approached the presented odour tube, the fifty-second presentation started, and it was quickly taken away after that time. For every trial, the length of time spent sniffing the provided odour tube was noted. If an animal could recognize and discriminate between various scents, it would be expected that its sniffing time would increase on the first exposure to each new scent and gradually decrease on subsequent exposures as the animal became used to it (Escanilla et al., 2010).

2.2.3.3 Food Retrieval with Simple Odour Discrimination

In the Food Retrieval with Simple Odor Discrimination (FRT & SOD), animals are subjected to food deprivation at a rate of 20g per day. The training incorporates a food reward, specifically Reese's Puffs cereal, into their daily feeding routine. The experimental setup involves preparing sponges by hollowing out the center from the top, using the green piece as a plug/cover, and hiding food inside the negative odour sponge. Before the trials, habituation takes place, including spending 10 minutes in the box on a day before starting and training the animals to eat food from the sponge. The animals are then gradually exposed to odour pairs, categorized as simple (SOD) such as almond vs. coconut. Trials are conducted by randomly switching the placements of positive (almond) and negative (coconut) sponges, each marked for identification. The animals must demonstrate odour discrimination by responding correctly to the placement of the positive sponge,

baited with a single piece of food while avoiding the negative sponge with hidden food. A trial is completed when a response is made, and the correct and incorrect responses are recorded. The animals progress to the next stage or finish training when they consistently achieve seventy percent correct responses or more over three consecutive days.

2.3 Tissue Processing

2.3.1 Perfusions

Transcardiac perfusions are systematically executed in a three-step procedure (Connor et al., 2009). Initially, a solution of phosphate-buffered saline containing Heparin sodium (10 units ml-1) was injected at a consistent rate of 50 ml per minute for forty-five seconds. Subsequently, a fixative solution consisting of 1% paraformaldehyde, 1.25% glutaraldehyde, and 0.02mM CaCl2 in 0.12M phosphate buffer (pH 7.3) was perfused at an initial rate of 50 ml per minute for ten minutes (500 ml) and then at a reduced rate of 25 ml per minute for an additional twenty minutes (500 ml). The third step involves the same fixative solution at twice the aldehyde concentration, administered at a rate of 25 ml/min for twelve minutes (300 ml). Throughout the entire process, all solutions are warmed to thirty-seven degrees Celsius and delivered via a peristaltic pump. Following perfusion, the animals are sealed in plastic bags and refrigerated for two hours at four degrees Celsius. The brain was subsequently extracted, placed in a vial mounted on a tissue rotator, and postfixed in the double-strength fixative at 4 degrees Celsius overnight. After roughly twenty-four hours, the double-strength fixative was replaced with Sorensen buffer (Appendix I). This protocol ensures optimal preservation and fixation of the biological specimens for subsequent analysis (Connor et al., 2009).

2.3.2 Locus Coeruleus Macrosection

The brains were placed in 0.1M Sorensen's phosphate buffer solution and sectioned at 700μm using a Pelco 102 Vibratome with injector carbon steel blades. The Rat Brain in Stereotaxic Coordinates 6th edition (Paxinos and Watson, 2014) was used to graphically assess the location and depth of coronal slices according to bregma (-9.48 to -10.44; Appendix II). The optimal 3-4 sections from the vibratome containing LC tissue were analyzed under the Olympus SZ61 dissecting microscope. Using a scalpel, the LC was dissected into squares and placed into labelled vials filled with 0.1M Sorensen's phosphate buffer solution (Appendix III).

2.3.3 Embedding

The tissue was embedded into an embedding medium for electron microscopy. The embedded tissue was placed into labelled gelatin capsules, followed by the addition of one hundred percent LR white resin. LR white resin is a hydrophilic acrylic resin of low viscosity with wide applications suitable for both light and electron microscopy. Resin polymerization was catalyzed using thermal curing. Capsules were heat-cured in an Isotemp 500 Series Laboratory Oven for forty-eight hours between fifty-five and sixty degrees Celsius (Appendix IV). The cured capsules were soaked in warm water until the gelatin melted off the resin which took approximately thirty minutes (Appendix V).

2.3.4 Trimming and Tissue Cutting

Resin blocks were trimmed using the Leica EM Trim. The flat face of the tissue was reduced into the shape of a trapezoid so that orientation positioned the 4th ventricle near the short parallel face of the trapezoid (Appendix VI). Trimmed resin blocks were locked in the Leica Ultracut R chuck. A slice of 1000nm thickness was cut from each LC block using a glass knife (Appendix VII; Appendix VIII). The sections were then stained with a Toluidine Blue O stain (Appendix IX). Stained LC slides were viewed under the Leica DMLB light microscope. The location of the LC

was determined based on the presence of cell clusters ventral to the 4th ventricle using The Rat Brain in Stereotaxic Coordinates 6th edition (Paxinos and Watson, 2014). Original resin blocks were returned to the Leica EM Trim, where the tissue was removed until the face exclusively displayed LC tissue.

Re-trimmed blocks were returned to the Leica Ultracut R. Silver to pale blonde coloured slices were obtained by setting the parameters to cut at 60-65nm thickness on the DiATOME 45° diamond knife. Once a ribbon of tissue slices was formed on top of the water basin, a cotton swab dipped in chloroform was gently hovered over the tissue surface. Approximately three copper 300-line square mesh grids were tapped onto tissue ribbons of four to five slices. Copper grids were laid tissue side up onto a grid-grid to airdry and then placed systematically in a grid holding box (Appendix X).

The diamond knife was exchanged for a glass knife and ten slices of 1000nm thickness were sliced from the resin blocks. The thick sections were cut to ensure random sampling throughout the entire LC structure and to ensure a new set of cells. The thin-cutting procedure was repeated twice for a total of nine copper grids per brain.

2.3.5 Imaging

Copper grids were placed into a Philips CM 10 TEM. Parameters were set and confirmed on the TEM before insertion of the copper grids (emission current: 2, high tension: 60kV, Ion Getter Pump Position 3: equal to or less than 40, configuration: tungsten, with filament set to 20). Three cells were randomly selected from each depth conditional on the presence of a clear nucleus and cell body that is not covered by a grid line. An image was first taken of the entire cell body around 2300X-10500X magnification as dependent on cell size. Then, images were captured of

mitochondrial profiles in the cell body at 19000X-25000X magnification, carefully ensuring all mitochondrial profiles were accounted for but had not been captured twice.

2.3.6 Imaging Analysis

Images were analyzed using ImageJ software version IJ1 as described in Schneider (2012). A total of eight variables were analyzed per mitochondrial profile. The shape was recorded as either round, elongated or dumbbell-in shape. A scale was used from 0-2 for damage to cristae in Figure 2 below (0 – no damage, 1 – slight damage, 2 – lots of damage). The area of each profile was calculated in nanometers squared (nm^2) using the free-hand lasso tool on ImageJ. Proximity to the nucleus in nm was measured with a straight line from the outer mitochondrial membrane to the adjacent nuclear membrane. Mitochondrial membrane integrity was observed by classifying each outer membrane as broken in a yes or no observation. Mitochondrial membranes that pinched together were recorded as a binary yes or no. A swollen appearance was also recorded as yes or no. All of these are depicted in Figure 2 and Figure 17.

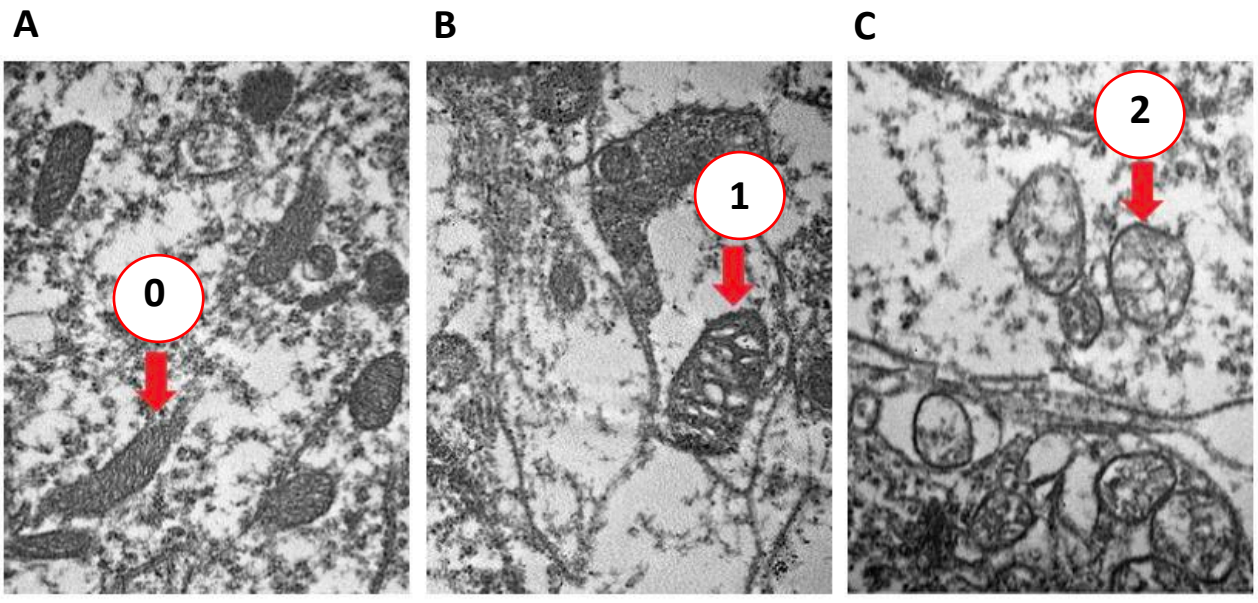

Figure 2. Transmission Electron Microscopy images of mitochondria cristae derangement levels at 25000x magnification. A) Mitochondria cristae derangement level 0 (no derangement). B) Mitochondria cristae derangement level 1 (low derangement). C) Mitochondria cristae derangement level 2 (high derangement).

2.3.7 Statistical Analysis

The statistical software used for this analysis was through Origin Lab interface. The chosen alpha value was $\alpha = 0.05$ for the multiple one-way ANOVA (analysis of 16 variance statistical test) tests followed by posthoc Tukey tests, to statistically analyze differences in mitochondrial profile areas (continuous variable; nm^2), morphology, membrane integrity, cristae derangement levels, total counts, along with general behaviour, learning and memory cognitive tasks between the two experimental and the control group.

3.0 Results

3.1 General Behaviour Results

3.1.1 Sucrose Preference Task

The htauE14 and htau experimental groups had no significant difference in comparison to the GFP control group in the sucrose preference task. A one-way ANOVA revealed that there was no significant effect of the virus on sucrose preference ($F(2,24) = 1.78922$, $p = 0.19056$, Figure 3)

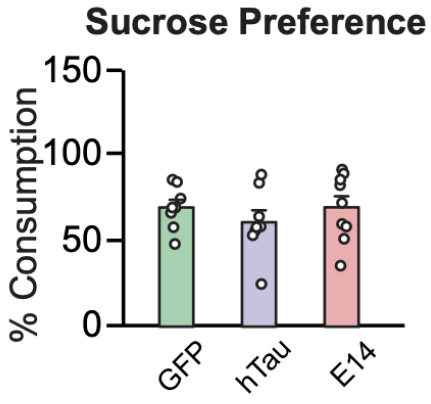

.

Figure 3. Summary of percentage of total sucrose consumed in 24 hours during the sucrose preference test. The htauE14 and htau-infused animals had no significant difference in the sucrose preference task in comparison to the GFP-infused animals.

3.1.2 Marble Burying Task

There was no significant difference between any of the experimental or control groups in the marble burying task. A one-way ANOVA revealed no significant main effect of the virus on number of marbles buried ($F(2,24) = 0.85636$, $p = 0.43839$, Figure 4).

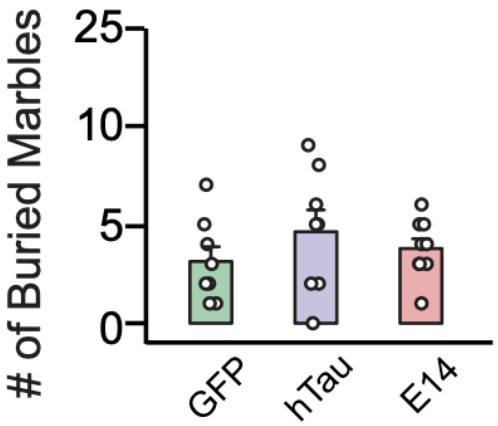

Figure 4. Summary of number of marbles buried during the marble burying test. The htauE14, htau and GFP animals showed no significant differences in marbles buried.

3.1.3 Elevated Plus Maze

There was no significant difference between any of the experimental or control groups in the elevated plus maze. A one-way ANOVA revealed no significant main effects of the virus on the percentage of time spent in closed arms during the EPM trial ($F(2,24) = 1.28577$, $p = 0.29641$, Figure 5).

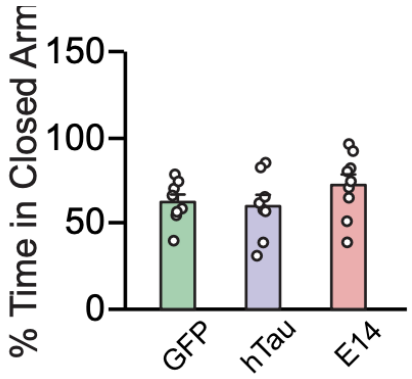

Figure 5. Summary of EPM results, percent of time spent in closed arms during the EPM trial. Control, htau and htauE14-infused animals had no significant differences in time spent in the closed arm.

3.1.4 Open Field Maze Task

All animals demonstrated equivalent activity and exploration in the OFM than controls through distance travelled, time spent rearing, and time spent freezing. A one-way ANOVA indicated no significant main effect of the virus on the distance travelled in the OFM ($F(2,24) = 0.04093$, $p = 0.95997$). A one-way ANOVA revealed no significant main effects of the virus on time spent rearing during the OFM ($F(2,24) = 0.74063$, $p = 0.48833$). Lastly, a one-way ANOVA revealed no significant main effect of the virus on the amount of time spent freezing during the OFM trial ($F(2,24) = 2.17963$, $p = 0.13689$, Figure 6).

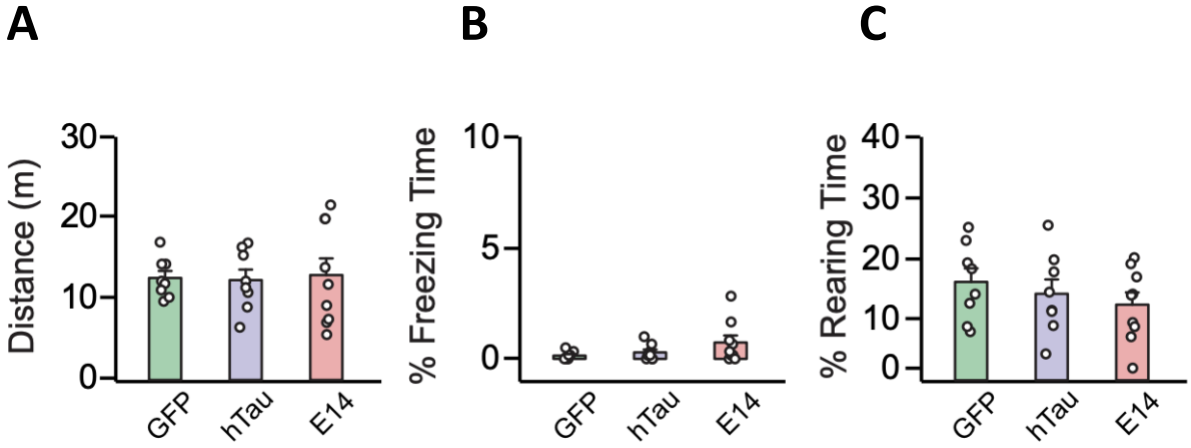

Figure 6. Summary of OFM results. A) All groups travelled equivalent distances in the distance travelled part of the OFM. B) All groups had similar freezing in the OFM trial. C) All groups spent similar times rearing in the OFM trial.

3.2 Learning Behaviour Results

3.2.1 Spontaneous Location Recall Task

The htauE14-infused animals were impaired compared to control and htau virus-infused animals in recognizing the novel location object. A one-way ANOVA showed a significant main effect of the htauE14 and htau virus compared to the control on the discrimination index for the SLR task($F(2,24) = 17.83865$, $p < 0.001$). Post-hoc Tukey test showed differences between GFP and htauE14 ($p = 2.08392e\text{-}5$). The post-hoc Tukey test also showed differences between htau and htauE14 ($p = 0.00221$, Figure 7).

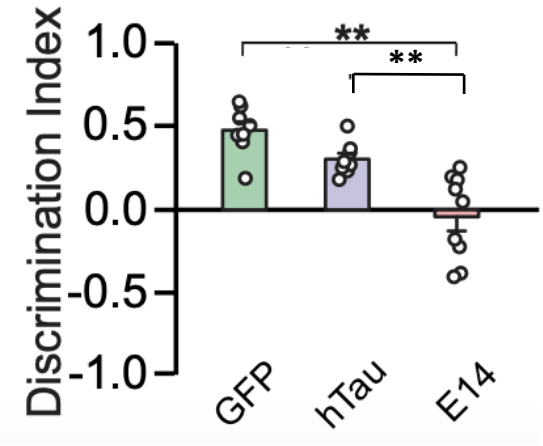

Figure 7. Summary of SLR test results. ** indicates min. $p < 0.01$. Discrimination index values from the SLR test. Control-infused animals spent more time with the novel object location than htauE14 virus-infused animals. Similarly, htau virus-infused animals spent more time in the novel object location in comparison to htauE14 virus-infused animals.

3.2.2 Odour Detection and Discrimination Task

The htauE14-infused animals were impaired at discriminating between similar odours compared to controls and htau-infused animals. A one-way ANOVA revealed a significant main effect of the virus on the ODAD discrimination index ($F(2,24) = 4.0882$, $p = 0.03092$). The posthoc Tukey test revealed that there is a difference between the GFP and htauE14 ($p = 0.02642$, Figure 8)

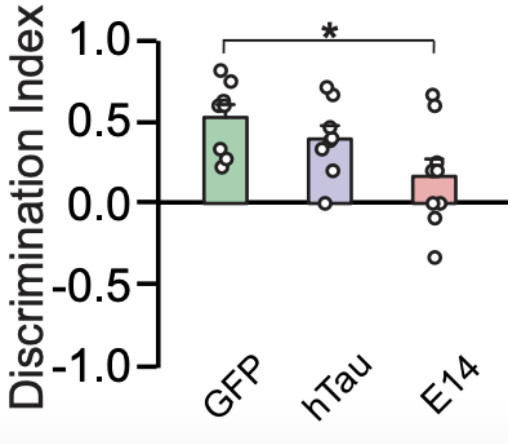

Figure 8. Summary of discrimination index values from the ODAD test. * indicates min. $p < 0.05$. The htauE14-infused animals were impaired compared to control and htau-infused animals at discriminating between similar odours.

3.2.3 Food Retrieval with Simple Odour Discrimination Task

The htauE14-infused animals were slower at learning and discriminating between odours compared to controls and htau-infused animals. A two-way ANOVA revealed no significant interaction between the days and groups in the ODAD task ($F_{114,154} = 0.929$, $p = 0.529$, Figure 9).

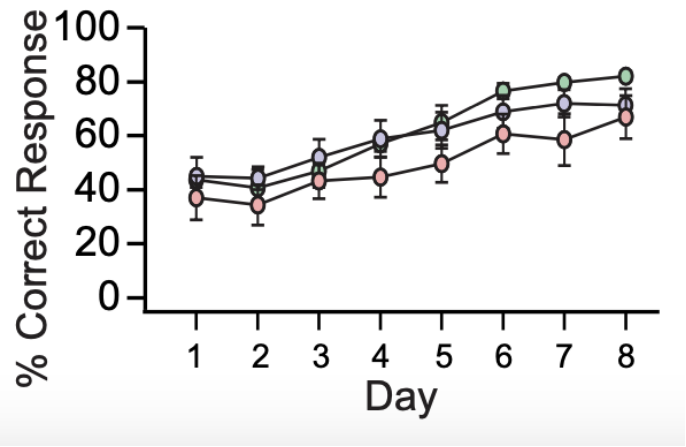

Figure 9. Summary of values from the Food Retrieval with Simple Odour Discrimination test. The htauE14-infused animals were slower to learn and discriminate odours compared to control-infused animals. Here the green represents the GFP group, the light purple represents the htau group and the red represents the htauE14 group.

3.3 TEM Results

The analysis for these TEM results was based on the cells counted per animal. There were three cells analyzed per depth analyzed and there were three depths total per animal, meaning one brain had nine cells to represent one animal. This then increased our N values to allow for a deeper analysis of the mitochondrial results.

Neurons were selected as per Nahirney and Tremblay (2021). The neuron had to contain a large euchromatic nucleus with centrally located nucleoli, and a large primary dendrite leaving the cell body (Nahirney and Tremblay, 2021). Satellite cells (microglia and oligodendrocyte precursor cells) typically have a smaller ovoid nucleus, and glial cells depict a darker, granule-dense cell body (Nahirney and Tremblay, 2021).

3.3.1 Mitochondria Cristae Derangement

The htauE14-infused animals had increased levels of damaged mitochondrial cristae compared to controls and htau-infused animals. A one-way ANOVA revealed a significant main effect of the virus on the cristae derangement levels ($F(2,161) = 7.53125$, $p < 0.01$). The posthoc Tukey test revealed a difference between GFP and the htauE14 group as well as between the tau and htauE14 groups ($p = 0.00268$ and $p = 0.00193$, respectively, Figure 10)

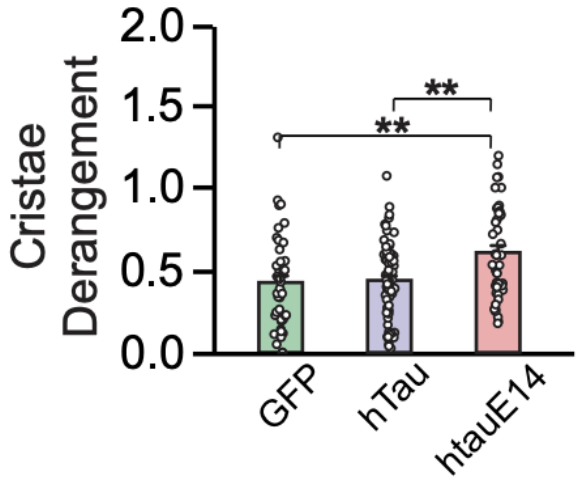

Figure 10. Summary of mitochondrial cristae derangement. ** indicates min. $p < 0.01$. The index score = (0 x N1 + 1 x N2 + 2 x N3)/(N1+N2+N3). Where N represents the number of mitochondria; 0-2 represents the degree of derangement, with 2 being the highest, 0 is no derangement. The htauE14-infused animals were significantly more impaired compared to control and htau-infused animals.

3.3.2 Mitochondria Membrane Integrity

The htauE14-infused animals had lower levels of mitochondrial membrane integrity compared to controls and htau-infused animals. A one-way ANOVA revealed a significant main effect of the virus on the membrane integrity ($F(2,161) = 4.90188$, $p= 0.00859$). The post-hoc Tukey test revealed a difference between GFP and the htauE14 group as well as between the htau and htauE14 groups ($p = 0.01764$ and $p = 0.01761$, respectively, Figure 11).

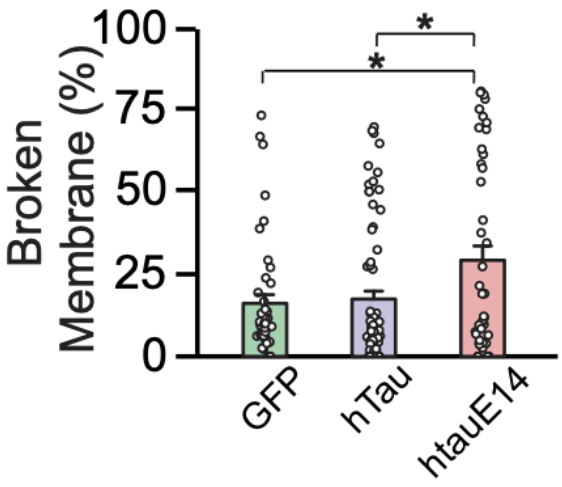

Figure 11. Summary of values from mitochondrial membrane integrity levels * indicates min. $p < 0.05$. The htauE14-infused animals had highly impaired mitochondrial membranes compared to control and htau-infused animals.

3.3.3 Mitochondria Morphology

Controls had significantly more round-shaped mitochondria in comparison to the htau and htauE14 virus-infused animals. Meanwhile, htauE14 virus-infused animals had a significantly greater number of elongated-shaped mitochondria compared to controls. A one-way ANOVA revealed a significant main effect of the virus on the overall mitochondria ($F(2,161) = 4.90188$, $p= 0.00859$). The post-hoc Tukey test showed a difference for the round mitochondria between the GFP and htau groups along with between the GFP and htauE14 groups ($p = 0.01135$ and $p = 5.41713e-6$). The post-hoc Tukey test also revealed a difference in elongated mitochondria between the GFP and the htauE14 groups ($p = 0.02733$, Figure 12).

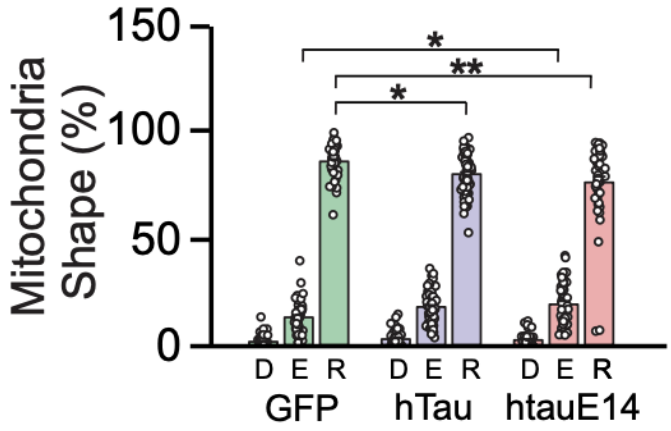

Figure 12. Summary of the morphology of the mitochondria. * indicates min $p < 0.05$, ** indicates min. $p < 0.01$. Controls had significantly more morphologically round mitochondria in comparison to the htau and htauE14 virus-infused animals. Meanwhile, htauE14 virus-infused animals had a significantly greater number of elongated mitochondria compared to control animals.

3.3.4 Mitochondria Fision and Fusion

The htauE14, htau and control virus-infused animals all demonstrated similar numbers of fission and fusion (pinching). A one-way ANOVA revealed no significant main effect of the virus on fission and fusion ($F(2,161) = 0.19436$, $p = 0.82356$, Figure 13).

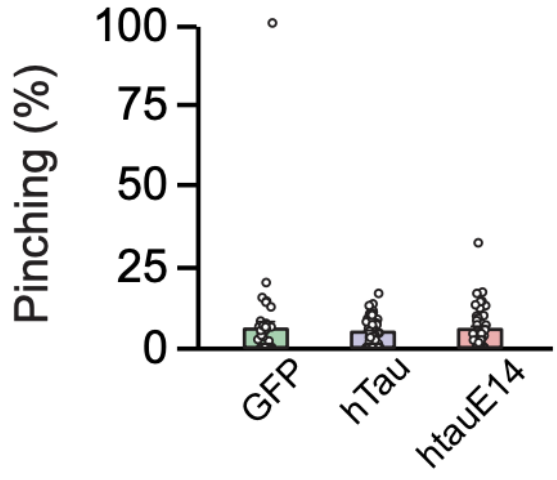

Figure 13. Summary of fission and fusion of mitochondria. The htauE14, htau and control virus-infused animals all demonstrated similar numbers of fission and fusion.

3.3.5 Mitochondria Distance to Nucleus

The htauE14, htau and control virus-infused animals were all relatively similar distances away from the nucleus. A one-way ANOVA revealed no significant main effect of the virus on the mitochondrial distance away from the nucleus ($F(2,161) = 1.46414$, $p = 0.23438$, Figure 14).

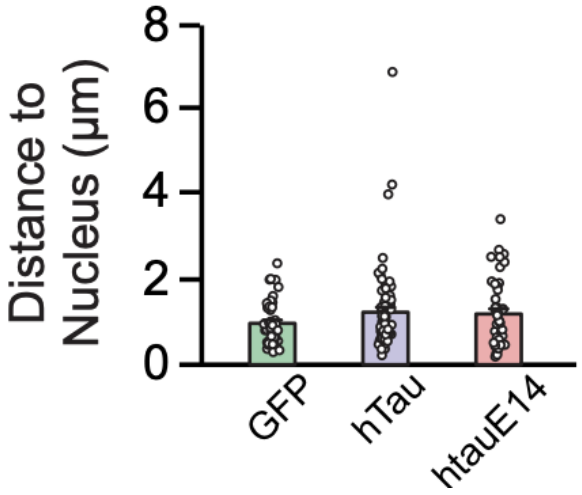

Figure 14. Summary of the mitochondrial distance from the nucleus. The htauE14, htau and control virus-infused animals all had relatively similar distances away from the nucleus.

3.3.6 Mean Mitochondrial Area

All animals demonstrated similar mitochondrial areas. A one-way ANOVA indicated no significant main effect of the virus on the mitochondrial areas ($F(2,161) = 2.49168$, $p = 0.086$, Figure 15).

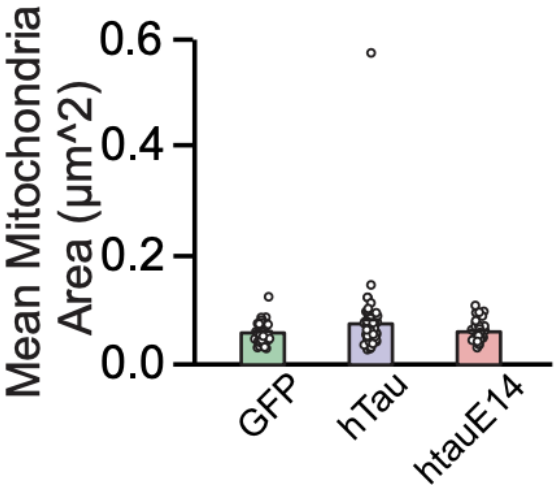

Figure 15. Summary of mean mitochondria areas. All animals demonstrated similar mitochondrial areas.

3.3.7 Total Mitochondrial Means

All animals demonstrated a similar number of total mitochondria in each group. A one-way ANOVA indicated no significant main effect of the virus on the total number of mitochondria ($F(2,161) = 1.24707$, $p = 0.29014$, Figure 16).

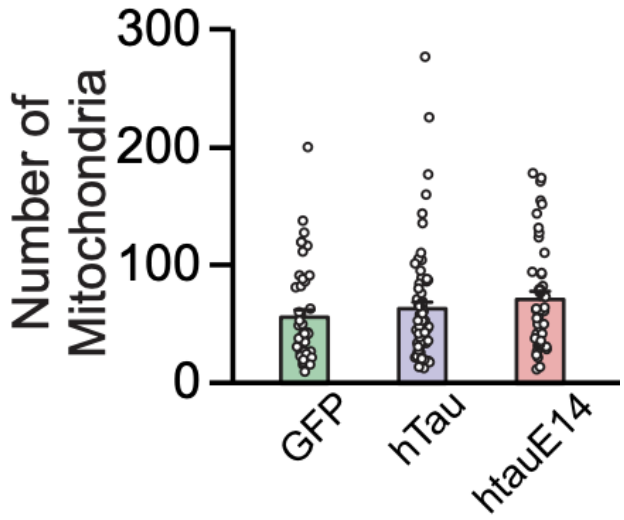

Figure 16. Summary of the total number of mitochondria in each group of animals. All animals demonstrated similar total numbers of mitochondria.

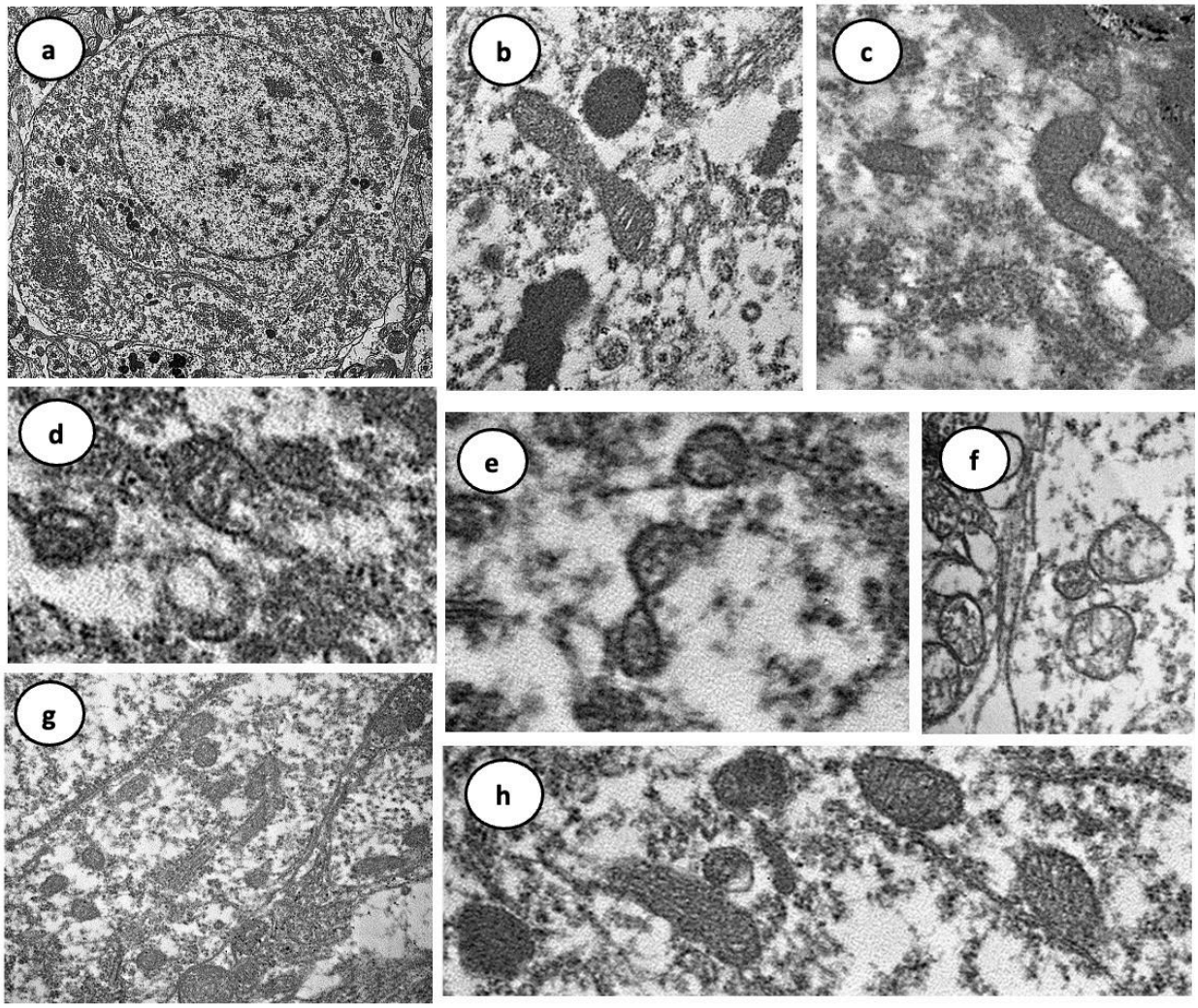

Figure 17. TEM image analysis. a) whole cell image b) dumbbell-shaped mitochondria c) elongated-shaped mitochondria d) broken outer membrane and cristae derangement e) pinching and round shaped mitochondria f) cristae derangement g) mitochondrial proximity to the nuclear membrane measured in nm h) healthy mitochondria.

3.3.8 Behaviour Tasks and TEM Correlation

A preliminary correlation analysis was performed however, no significant interactions were found. As we can see there is a trend between cristae derangement levels and spatial memory. When rodents depict more severe cristae derangement they have less spatial recognition and memory

ability. Therefore, there is a degree to which mitochondria deficiency and damage are related to behavioural deficits. This is an area where further research on aged and young AD animal models could be done.

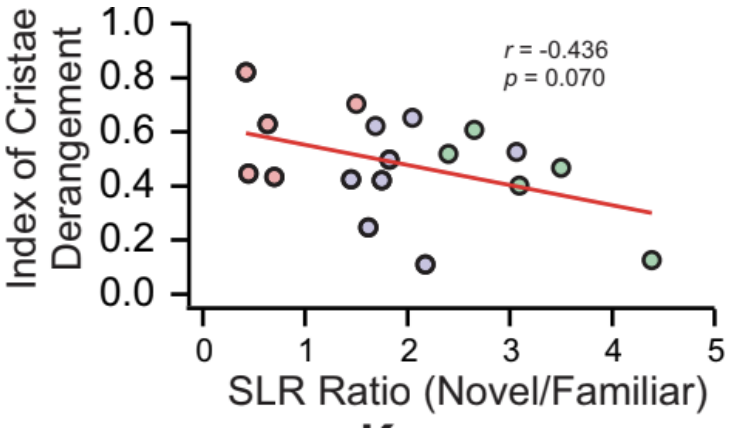

Figure 18. Cristae derangement and SLR Correlation. No significant interactions are shown.

4.0 Discussion

This study demonstrates that our pre-tangle tau pseudo phosphorylated virus-infused animal model (htauE14) created deficits in the behaviour of the animals, which includes diminishing their ability to make new spatial and olfactory memories. Additionally, these animals had increased morphological mitochondrial damage in comparison to the control and the human tau viruses-infused animals.

First, under the general behaviour tasks, the SPT did not show any significant difference among the three groups. A lower preference for sucrose water would be an indication of anhedonia, which is a lack of interest/enjoyment. This would then indicate depressive-like symptoms in the animals (Liu et al., 2018). However, in this study, there was no preference, therefore there were no signs of depression among the three groups of animals.

Next, the MBT demonstrated no significant differences amongst groups. Animals tend to bury more when possessing anxiety-like symptoms, therefore the animals in the study would bury more marbles if anxious (Archer et al., 1987). Since there was no difference observed between groups, no anxiety phenotype was observed by this task.

The EPM demonstrated no significant differences amongst groups. Animals spending more time in the closed arms of this maze would indicate a slightly higher prevalence of stress (Kraeuter et al., 2019). Since there was no difference observed between groups, no stress phenotype was observed by this task.

In the OFM test, all animals demonstrated equivalent activity and exploration to controls. This was measured through distance travelled, time spent rearing, and time spent freezing. No significant differences were discovered between any of the groups or any of the tests (distance travelled, freezing time and rearing time). Higher freezing and lower rearing times would indicate higher levels of anxiety and stress (Seibenhener & Wooten 2015). As there were no significant differences between the groups, no stress or anxiety phenotypes were observed.

Under learning behaviour tests, the SLR task demonstrated a significant difference between control animals, htau as well as htauE14 virus-infused animals. The htau and htauE14 virus-infused animals were not able to identify the differences between the novel and familiar objects' locations. This here indicates that our model does impair the memory-making and learning abilities of the animals (Bekinschtein et al., 2013).

Next, the ODAD had a significant difference between the control animals in comparison to the htauE14 virus-infused animals. The htauE14 had clear deficits in discriminating novel and familiar odours (Escanilla et al., 2010). This here again is a clear sign of memory and learning defects for the htauE14 model.

The last behaviour test was the FRD, which had no significant interactions between the days and the groups. There was no sign of memory or learning impairment throughout this task, all animals struggled to associate and learn to differentiate different odours.

Onto the electron microscopy imaging results. To begin, the mitochondrial cristae derangement had a significant difference between the htauE14 and both the control and the htau virus-infused animals. The htauE14 animals demonstrated a higher amount of damaged cristae in comparison to the other groups. According to Moreira and colleagues (2010), when there is evident evidence of mitochondrial damage, this would suggest neuronal damage. Numerous mitochondria appear enlarged and become structurally disorganized as the brain ages (Moreira et al., 2010). This potentially could be caused by both the incapacity of cells to eliminate oxidatively damaged structures as well as continuously undergoing oxidative stress; which causes oxidization of mitochondria (Moreira et al., 2010). Age-related declines in mitochondrial turnover lead to increased oxidative damage, the build-up of damaged organelles, a reduction in ATP production, the release of apoptotic factors, and ultimately, cell death (Moreira et al., 2010).

Consistently, the membrane integrity of the analyzed mitochondria also showed significant differences between the control group, the htau virus-infused as well as between the control group with the htauE14 virus-infused animal. Ruptures to either the outer or inner mitochondrial membrane decrease the organelles' permeability (Sesso et al., 2012). Therefore, increasing the risk of allowing damage into the organelle to further cause cristae degradation, swelling and mitophagy (Sesso et al., 2012).

In this study, we did not perform 3D reconstructions of all of the synapses studied, so we cannot draw firm conclusions about mitochondrial morphology, but we did observe mitochondrial

profiles in single sections that had abnormal morphology. There was a clear observation of higher round mitochondria in all groups, as well as a significant difference between the GFP virus-infused animals and both the htau and htauE14 virus-infused animals. The GFP group had more round-shaped mitochondria compared to the other two groups. There was also a significant difference between the GFP virus-infused animals and the htauE14 virus-infused animals, which had more elongated shaped mitochondria than the control group. In a study conducted by Brandt and colleagues, older mitochondria in heart and liver cells were unusually long and thin, while their cristae assumed a variety of non-standard shapes (Brandt et al., 2017). The morphology of the mitochondrial network is sustained by continuous rounds of fusion and fission (Szabo et al., 2020). Consequently, the balance between the set of opposite processes modulates mitochondrial number, shape and size. While increased fusion generates elongated, interconnected mitochondria, enhanced fission promotes mitochondrial fragmentation (Szabo et al., 2020). This plastic adaptation is particularly essential in neurons that are highly polarized cells (Szabo et al., 2020). These findings and theories may lead to a possible new biomarker for AD.

The number of mitochondria observed in fission or fusion states between the three groups had no significant differences. There were low counts observed across all groups. Fission and fusion are two opposing processes that mitochondria continuously go through. According to Moreira and colleagues (2010), the disturbance of this dynamic equilibrium could signal cellular damage or death as well as play a role in neurodegenerative diseases. They also state that the breakdown of mitochondria is a strictly controlled process, and these organelles are mostly shielded from non-specific autophagic degradation (Moreira et al., 2010). Altered fission or fusion of mitochondria in AD could further explain a reduction in mitochondria present at presynaptic

sites, this could be accounted for by an increase in mitochondrial turnover by mitophagy (Pickett et al., 2018).

The distance from the nuclear membrane to the outer mitochondrial membrane had little to no significant differences between the three groups. Synaptic mitochondria play a potentially important role in synapse degeneration in AD (Pickett et al., 2018). The results from a study conducted by Pickett and colleagues show region-specific changes in synaptic mitochondria in AD and support the idea that the transport of mitochondria to presynaptic terminals or synaptic mitochondrial dynamics may be altered in AD (Pickett et al., 2018). The role of mitochondria in metabolism is crucial for providing the necessary energy required for neurotransmitter release at the presynapse. Since the synapse is a site of high-energy demand, mitochondria must be trafficked to this location (Pickett et al., 2018). Tau plays a crucial role in binding and stabilizing microtubules required for this anterograde transport of mitochondria (Götz et al., 2007). It has been suggested that pathological tau may interfere with this trafficking process resulting in impaired anterograde transport of cargo (Götz et al., 2007). The overexpression of tau inhibits anterograde mitochondrial transport and disrupts mitochondrial distribution in neurons, resulting in perinuclear clumping in the soma (Pickett et al., 2018). Tau overexpression in neurons has also been proven to increase the pausing frequency of mitochondria movement by sixteen percent. (Shahpasandet al., 2012). Our findings did not show significance however, more research should be performed to solidify these statements. There is the possibility that mitochondria clumping and/or frequency near the soma would possibly indicate AD or damage to the neuron.

This study did not directly analyze neural death or stress however, from our previous studies we found no cell loss (by Nissl) when AAV was infused three months, and the histology was done at eight months post-infusion (Ghosh et al., 2019). Also, Omoluabi and colleagues

(2020), showed that AC3 (a cell apoptosis marker) was not found different in E14 vs GFP control rats, only LC tonic stimulation increased it. These results suggest no cell loss, but neurodegeneration was present (e.g. LC axonal degeneration).

The mean area of the mitochondria across all groups is relatively the same, therefore showing no significant differences. The rupture of the outer membrane leads to the loss of selective permeability which causes an influx of cytoplasmic fluids into the inner membrane and matrix (Sesso et al., 2012). This in turn leads to mitochondrial swelling/enlargements (Sesso et al., 2012). An occurrence of functionally insufficient enlarged mitochondria is associated with aging (Terman et al., 2010) or oxidative stress (Redpath et al., 2013; Kamogashira et al., 2017). Therefore, more enlarged/swollen mitochondria could be a sign of AD. As our research did not include creating 3-D models of mitochondria we could not make conclusions about whether or not the mitochondria were swollen. This is an area where more research could be done.

The number of mitochondria across each group is very similar, therefore showing no significant differences between the groups. Mitochondria are the first cellular compartments to be affected and respond to any stimuli (Devin et al., 2019). In a study conducted by Shults and colleagues (2019), it was concluded that an increased number of small round mitochondria would be an indication of increased fission. Drawing any conclusions from the mitochondria count would be biased as a full stereological method would be needed to create full 3D models of the neurons to fully conclude the total numbers. The stereological methods provide accurate and unbiased quantification of mitochondria from 2D sections (Duranova et al., 2020).

4.1 Summary of Main Findings

Overall, the most prominent findings from this study were the clear learning and memory deficits of the htauE14 animal model through the spatial discrimination task as well as the odour

discrimination task. The animals were less able to discriminate between both novel and familiar object locations and odours. The htauE14 animal models also depicted higher levels of cristae derangement as well as increased frequency of broken mitochondrial membranes. Changes in mitochondrial ultrastructure occur in response to cellular stress contributing to a broad spectrum of pathological conditions (Duraanova et al., 2020). All in all, this data leads credence to the idea that mitochondrial damage is elevated in vulnerable neurons in AD.

4.2 Limitations

All limitations were taken into consideration when analyzing the results of this study. Efforts were made to avoid experimenter bias, including following strict protocols during testing, video recording trials to verify results, and having a blind experimenter conduct the test when possible.

One limitation of the study was the sample size per group. There were between 8 and 9 animals per group. Some animals showed signs of hypoxia while analyzed under the electron microscope, therefore they had to be removed from the analysis. Hypoxia can occur when a perfusion is poorly done. Typically, when it is not performed quickly enough low blood oxygen levels are introduced to the brain too slowly. Increasing the sample sizes would increase the statistical power of the analyses conducted and potentially provide further insight into the factors being considered and their relationship to AD pathology.

In a study conducted by Hu and colleagues (2021), it was discovered that women had higher Braak stages and amyloid scores than men. Another interesting discovery was that in the cognitively intact elderly, women's entorhinal cortex accumulated more phosphorylated tau than amyloid beta proteins, in contrast to men (Hue et al., 2021). Typically, along the AD spectrum, women exhibit more pathological Tau biomarkers than men (Sundermann et al., 2020). There is

an obvious need to address sex differences by increasing the sampling number of both genders in AD research. As for this project, we used a mix of both, but not enough to measure sex as a variable.

Several organelles that were identified as mitochondria by their characteristic double membrane and dense matrix appeared to lack cristae entirely or the cristae were minimally developed. Many cristae were not connected to the intermembrane space and were, therefore, small vesicles surrounded by matrix. A previous study has identified mitochondria with spherical cristae, in others, they were concentric (Brandt et al., 2017). Therefore, to the best of our abilities, we made a judgment of what is and what is not considered mitochondria throughout our analysis.

The shape and size of the mitochondria also could be a limitation. The amount of swelling and the breaking of the inner membrane can also play a role in the shape and size of the mitochondria. The small protrusions of the inner membrane through the perforation in the outer membrane suggest that the initial rupture and the preceding intermembrane swelling were both localized and small (Sesso et al., 2012). Just before the rupture of the outer membrane, the permeability of both mitochondrial membranes increases where the localized intermembrane swelling forms (Sesso et al., 2012). It appears that although the selective permeability of the inner membrane was maintained in most cases, it allowed the entrance of sufficient fluid into the matrix to cause swelling (Sesso et al., 2012). The rupture of the outer membrane exposes the inner membrane which causes an impermeability transition to the cytoplasm. This is sufficient to produce the formation of a focal hernia of considerable size which also can alter the shape and size of the mitochondria (Sesso et al., 2012). Therefore, to the best of our abilities, we made a judgment of what is and what is not considered an intact mitochondrial membrane, and the shape/size of the mitochondria itself throughout our analysis.

4.3 Conclusion and Future Directions

Postmitotic cells, like neurons, are primarily affected by age-related mitochondrial damage because they are rarely or never replaced due to stem cell division or differentiation (Terman et al., 2010). The cell's factories for producing energy are mitochondria; when these organelles malfunction, the cell is deprived of ATP and produces more reactive oxygen species, which ultimately triggers apoptosis (Chistiakov et al., 2014). Defective mitochondria gradually accumulate due to autophagy and other cellular-degradation mechanisms are innately unable to fully eliminate damaged structures (Chistiakov et al., 2014). A growing population of defective and enlarged mitochondria are poorly autophagocytosed and do not fuse or exchange their contents with healthy mitochondria (Terman et al., 2010). As these alterations continue, there is an increase in oxidative stress and a decrease in ATP synthesis, both of which are ultimately detrimental to survival (Terman et al., 2010).

The mitochondrial cascade theory was put forth by Swerdlow and Khan (2009) to account for late-onset, sporadic AD. In summary, this theory proposes that amyloid-beta deposition, synaptic degeneration, and NFT formation in sporadic AD are primarily caused by mitochondrial dysfunction. A large body of research indicates that AD frequently results in mitochondrial dysfunction (Moreira et al., 2010).

According to Szabo and colleagues (2020), neuronal dysfunction, death, and dementia, such as Alzheimer's disease can result from changes in mitochondrial function caused by chemical or physical damage to these organelles. Furthermore, it is not unexpected that tau-induced mitochondrial dysfunction influences other cellular dysfunctions and vice versa; as mitochondria are not isolated self-autonomous organelles floating in the cytosol, but rather are intricately connected with other cellular compartments (Szabo et al., 2020).

Depletion of mitochondria at the synapse may be a synergistic mechanism contributing to synaptotoxicity, given that both tau and amyloid-beta are involved in disrupting anterograde mitochondrial transport (Pickett et al., 2018). This suggests that the mitochondria may become trapped in the dystrophies and are unable to reach the synaptic terminals (Pickett et al., 2018).

It is generally understood that elevated cellular stress is the potential cause of mitochondrial disruption at the synapse, which has been extensively studied in several neurodegenerative disease models (Pickett et al., 2018). According to Pickett and colleagues (2018) in the afflicted state, there is a decrease in the total number of mitochondria present in the presynaptic terminals. Disrupted anterograde transport could be one reason for this decrease in mitochondria (Pickett et al., 2018). All of these findings point to a region-specific reduction of synaptic mitochondria in the presynaptic terminals of AD. The conclusion is that mitochondrial axonal transport is compromised over long distances to synaptic terminals, specifically in vulnerable brain regions in AD (Pickett et al., 2018).

The results from this study are consistent with several studies suggesting that oligomeric species possess greater toxicity than aggregates. Deficits in axonal transport are possibly the cause of tau-induced deficiencies in mitochondrial distribution, which can lead to impaired neuronal and mitochondrial function, synaptic failure, and/or apoptosis.

An avenue worth exploring would be the mitochondria present at the pre-synaptic ends of the LC neurons that synapse at the hippocampus. Repeating a similar analysis to see whether there is a difference in total means of mitochondria across the different groups. As well as if there is less or more morphological damage to the organelles themselves. It is important to retain LC axonal transport to the terminals not only for the ability to provide noradrenaline and neurotrophins for post-synaptic components in neurons in the hippocampus (Ishida et al., 2000). The hippocampus

plays an important role in memory making, therefore being an ideal target for AD research. The hippocampal dentate gyrus consists of three layers, including the molecular layer, the granule layer and the polymorphic layer (Ishida et al., 2000). The polymorphic layer is one of the regions where the LC projects its axons and would be the ideal location to study under TEM (Ishida et al., 2000). The aim would be to identify and investigate mitochondrial age-dependent and AD changes in the projections from the LC to the hippocampal dentate gyrus.

References

Amuthan, G., Biswas, G., Ananadatheerthavarada, H. K., Vijayasarathy, C., Shephard, H. M., & Avadhani, N. G. (2002). Mitochondrial stress-induced calcium signalling, phenotypic changes and invasive behavior in human lung carcinoma A549 cells. *Oncogene,* 21(51), 7839–7849. https://doi.org/10.1038/sj.onc.1205983

Anderson, S., Bankier, A. T., Barrell, B. G., de Bruijn, M. H., Coulson, A. R., Drouin, J., Eperon, I. C., Nierlich, D. P., Roe, B. A., Sanger, F., Schreier, P. H., Smith, A. J., Staden, R., & Young, I. G. (1981). Sequence and organization of the human mitochondrial genome. *Nature*, 290(5806), 457–465. https://doi.org/10.1038/290457a0

Archer, T., Fredriksson, A., Lewander, T., & Söderberg, U. (1987). Marble burying and spontaneous motor activity in mice: interactions over days and the effect of diazepam. *Scandinavian Journal of Psychology*, 28, 242-249. doi: 10.1111/j.1467- 9450.1987.tb00761.x

Arnould, T. (2002). CREB activation induced by mitochondrial dysfunction is a new signalling pathway that impairs cell proliferation. *The EMBO Journal*, 21(1), 53–63. https://doi.org/10.1093/emboj/21.1.53

Barbier, P., Zejneli, O., Martinho, M., Lasorsa, A., Belle, V., Smet-Nocca, C., Tsvetkov, P. O., Devred, F., & Landrieu, I. (2019). Role of tau as a microtubule-associated protein: Structural and functional aspects. *Frontiers in Aging Neuroscience*, 11. https://doi.org/10.3389/fnagi.2019.00204

Bekinschtein, P., Kent, B. A., Oomen, C. A., Clemenson, G. D., Gage, F. H., Saksida, L. M., & Bussey, T. J. (2013). BDNF in the dentate gyrus is required for consolidation of "Pattern-Separated" Memories. *Cell Reports*, 5(3), 759-768. doi: 10.1016/j.celrep.2013.09.027

Bierer, L. M., Hof, P. R., Purohit, D. P., Carlin, L., Schmeidler, J., Davis, K. L., & Perl, D. P. (1995). Neocortical neurofibrillary tangles correlate with dementia severity in

Alzheimer's disease. *Archives of Neurology*, 52(1), 81–88. https://doi.org/10.1001/archneur.1995.00540250089017

Binder, L. I., Frankfurter, A., & Rebhun, L. I. (1985). The distribution of tau in the mammalian central nervous system. *Journal of Cell Biology*, 101, 1371-1378. doi: 10.1083/jcb.101.4.1371

Biswas, G. (1999). Retrograde ca2+ signaling in C2C12 skeletal myocytes in response to mitochondrial genetic and metabolic stress: A novel mode of inter-organelle crosstalk. *The EMBO Journal,* 18(3), 522–533. https://doi.org/10.1093/emboj/18.3.522

Braak, H., Thal, D. R., Ghebremedhin, E., & Del Tredici, K. (2011). Stages of the pathologic process in Alzheimer's disease: Age categories from 1 to 100 years. *Journal of Neuropathology and Experimental Neurology*, *70*(11), 960–69. https://doi.org/10.1097/NEN.0b013e318232a379

Brandt, T., Mourier, A., Tain, L. S., Partridge, L., Larsson, N.-G., & Kühlbrandt, W. (2017). Changes of mitochondrial ultrastructure and function during ageing in mice and drosophila. *eLife*, 6. https://doi.org/10.7554/elife.24662

Celsi, F., Pizzo, P., Brini, M., Leo, S., Fotino, C., Pinton, P., & Rizzuto, R. (2009). Mitochondria, calcium and cell death: A deadly triad in neurodegeneration. *Biochimica et Biophysica Acta (BBA) - Bioenergetics,* 1787(5), 335–344. https://doi.org/10.1016/j.bbabio.2009.02.021

Cid-Castro, C., Hernández-Espinosa, D. R., & Morán, J. (2018). Ros as regulators of mitochondrial dynamics in neurons. *Cellular and Molecular Neurobiology*, 38(5), 995–1007. https://doi.org/10.1007/s10571-018-0584-7

Connor, S., Bloomfield, J., LeBoutillier, J. C., Thompson, R. F., Petit, T. L., & Weeks, A. C. (2009). Eyeblink conditioning leads to fewer synapses in the rabbit cerebellar cortex. *Behavioral Neuroscience*, 123(4), 856–862. https://doi.org/10.1037/a0016370

Cortopassi, G. A., & Arnheim, N. (1990). Detection of a specific mitochondrial DNA deletion in tissues of older humans. *Nucleic Acids Research*, 18(23), 6927–6933. https://doi.org/10.1093/nar/18.23.6927

Chistiakov, D. A., Sobenin, I. A., Revin, V. V., Orekhov, A. N., & Bobryshev, Y. V. (2014). Mitochondrial aging and age-related dysfunction of mitochondria. *BioMed Research International*, 1–7. https://doi.org/10.1155/2014/238463

Counts, S. E., & Mufson, E. J. (2010). Noradrenaline activation of neurotrophic pathways protects against neuronal amyloid toxicity. *Journal of Neurochemistry*, 113(3), 649–660. https://doi.org/10.1111/j.1471-4159.2010.06622.x

Duranova, H., Valkova, V., Knazicka, Z., Olexikova, L., & Vasicek, J. (2020). Mitochondria: A worthwhile object for ultrastructural qualitative characterization and quantification of cells at physiological and pathophysiological states using conventional transmission electron microscopy. *Acta Histochemica,* 122(8), 151646. https://doi.org/10.1016/j.acthis.2020.151646

De Strooper, B., Saftig, P., Craessaerts, K., Vanderstichele, H., Guhde, G., Annaert, W., Von Figura, K., & Van Leuven, F. (1998). Deficiency of presenilin-1 inhibits the normal cleavage of amyloid precursor protein. *Nature*, 391, 387-390. doi: 10.1038/34910

Devin, A., Bouchez, C., Molini´ e, T., David, C., Duvezin-Caubet, S., Rojo, M., Mourier, A., Averet, M., Rigoulet, M. (2019). Mitochondria: Ultrastructure, dynamics, biogenesis and main functions. In mitochondria in obesity and type 2 diabetes. *Academic Press*, 3–32. https://doi.org/10.1016/B978-0-12-811752-1.00001-8.

Duchen, M. R. (2000). Mitochondria and calcium: From cell signalling to cell death. *The Journal of Physiology,* 529(1), 57–68. https://doi.org/10.1111/j.1469-7793.2000.00057.x

Escanilla, O., Arrellanos, A., Karnow, A., Ennis, M., & Linster, C. (2010). Noradrenergic modulation of behavioral odor detection and discrimination thresholds in the olfactory bulb. *European Journal of Neuroscience,* 32, 458-468. doi: 10.1111/j.1460- 9568.2010.07297.x

Ercan-Herbst, E., Ehrig, J., Schöndorf, D. C., Behrendt, A., Klaus, B., Ramos, B. G., Oriol, N. P., Weber, C., & Ehrnhoefer, D. E. (2019). A post-translational modification signature defines changes in soluble tau correlating with oligomerization in early stage Alzheimer's disease brain. *Acta Neuropathologica Communications*, 7(192). doi: 10.1186/s40478-019-0823-2

Esparza, T. J., Gangolli, M., Cairns, N. J., & Brody, D. L. (2018). Soluble amyloid-beta buffering by plaques in Alzheimer disease dementia versus high-pathology controls. *PLOS ONE*, 13(7). https://doi.org/10.1371/journal.pone.0200251

Friedman, J. R., & Nunnari, J. (2014). Mitochondrial form and function. *Nature,* 505(7483), 335–343. https://doi.org/10.1038/nature12985

Ghosh, A., Torraville, S. E., Mukherjee, B., Walling, S. G., Martin, G. M., Harley, C. W., & Yuan, Q. (2019). An experimental model of Braak's pretangle proposal for the origin of Alzheimer's disease: the role of locus coeruleus in early symptom development. *Alzheimer's Research and Therapy,* 11(1). doi: 10.1186/s13195-019-0511-2

Goedert, M., Spillantini, M. G., Jakes, R., Rutherford, D., & Crowther, R. A. (1989). Multiple isoforms of human microtubule-associated protein tau: Sequences and localization in neurofibrillary tangles of Alzheimer's disease. *Neuron*, 3(4), 519–526. https://doi.org/10.1016/0896-6273(89)90210-9

Goedert, M. (1993). Tau protein and the neurofibrillary pathology of Alzheimer's disease. *Trends in Neurosciences*, 16(11), 460–465. https://doi.org/10.1016/0166-2236(93)90078-z

Götz, J., Deters, N., Doldissen, A., Bokhari, L., Ke, Y., Wiesner, A., Schonrock, N., & Ittner, L. M. (2007). A decade of tau transgenic animal models and beyond. *Brain Pathology*, 17(1), 91–103. https://doi.org/10.1111/j.1750-3639.2007.00051.x

Grudzien, A., Shaw, P., Weintraub, S., Bigio, E., Mash, D. C., & Mesulam, M. M. (2006). Locus coeruleus neurofibrillary degeneration in aging, mild cognitive impairment and early Alzheimer's disease. *Neurobiology of Aging*, 28(3), 327–335. https://doi.org/10.1016/j.neurobiolaging.2006.02.007

Harman, D. (1972). The biologic clock: The mitochondria? *Journal of the American Geriatrics Society*, 20(4), 145–147. https://doi.org/10.1111/j.1532-5415.1972.tb00787.x

Hatanpää, K., Brady, D. R., Stoll, J., Rapoport, S. I., & Chandrasekaran, K. (1996). Neuronal activity and early neurofibrillary tangles in Alzheimer's disease. *Annals of Neurology,* 40(3), 411–420. https://doi.org/10.1002/ana.410400310

Himmler, A., Drechsel, D., Kirschner, M. W., & Martin, D. W. (1989). Tau consists of a set of proteins with repeated C-terminal microtubule-binding domains and variable N-terminal domains. *Molecular and Cellular Biology*, 9(4), 1381–1388. https://doi.org/10.1128/mcb.9.4.1381-1388.1989

Hoover, B. R., Reed, M. N., Su, J., Penrod, R. D., Kotilinek, L. A., Grant, M. K., Pitstick, R., Carlson, G. A., Lanier, L. M., Yuan, L.-L., Ashe, K. H., & Liao, D. (2010). Tau mislocalization to dendritic spines mediates synaptic dysfunction independently of neurodegeneration. *Neuron*, 68, 1067-1081. doi: 10.1016/j.neuron.2010.11.030

Hotka, M., Cagalinec, M., Hilber, K., Hool, L., Boehm, S., & Kubista, H. (2020). L-type ca 2+ channel–mediated ca 2+ influx adjusts neuronal mitochondrial function to physiological and pathophysiological conditions. *Science Signaling*, 13(618). https://doi.org/10.1126/scisignal.aaw6923

Hu, Y., Boonstra, J., McGurran, H., Stormmesand, J., Sluiter, A., Balesar, R., Verwer, R., Swaab, D., & Bao, A. (2021). Sex differences in the neuropathological hallmarks of Alzheimer's disease: focus on cognitively intact elderly individuals. *Neuropathology and Applied Neurobiology,* 47, 958-966. doi: 10.1111/nan.12729

Iba, M., McBride, J. D., Guo, J. L., Zhang, B., Trojanowski, J. Q., & Lee, V. M.-Y. (2015). Tau pathology spread in PS19 tau transgenic mice following Locus Coeruleus (LC) injections of synthetic tau fibrils is determined by the LC's afferent and Efferent Connections. Acta Neuropathologica, 130(3), 349–362. https://doi.org/10.1007/s00401-015-1458-4

Ishida, Y., Shirokawa, T., Miyaishi, O., Komatsu, Y., & Isobe, K. (2000). Age-dependent changes in projections from locus coeruleus to hippocampus dentate gyrus and frontal cortex. *European Journal of Neuroscience*, 12(4), 1263–1270. https://doi.org/10.1046/j.1460-9568.2000.00017.x

Jack, C. R., Knopman, D. S., Jagust, W. J., Shaw, L. M., Aisen, P. S., Weiner, M. W., Petersen, R. C., & Trojanowski, J. Q. (2010). Hypothetical model of dynamic biomarkers of the alzheimer's pathological Cascade. *The Lancet Neurology*, 9(1), 119–128. https://doi.org/10.1016/s1474-4422(09)70299-6

Jadiya, P., Kolmetzky, D. W., Tomar, D., Di Meco, A., Lombardi, A. A., Lambert, J. P., Luongo, T. S., Ludtmann, M. H., Praticò, D., & Elrod, J. W. (2019). Impaired mitochondrial calcium efflux contributes to disease progression in models of Alzheimer's disease. *Nature Communications,* 10(1). https://doi.org/10.1038/s41467-019-11813-6

Jang, J. Y., Blum, A., Liu, J., & Finkel, T. (2018). The role of mitochondria in aging. *Journal of Clinical Investigation,* 128(9), 3662–3670. https://doi.org/10.1172/jci120842

Jellinger, K. A. (2020). Neuropathological assessment of the Alzheimer's spectrum. *Journal of Neural Transmission,* 127(9), 1229–1256. https://doi.org/10.1007/s00702-020-02232-9

Ji, W., An, K., Wang, C., & Wang, S. (2022). Bioinformatics analysis of diagnostic biomarkers for Alzheimer's disease in peripheral blood based on sex differences and support vector machine algorithm. *Heredities*, *159*(1), 1–16. https://doiorg.roxy.nipissingu.ca/10.1186/s41065-022-00252-x

Kamogashira, T., Hayashi, K., Fujimoto, C., Iwasaki, S., Yamasoba, T. (2017). Functionally and morphologically damaged mitochondria observed in auditory cells under senescence-inducing stress. *NPJ Aging Mech. Dis*. 3 (1), 1–11. https://doi.org/ 10.1038/s41514-017-0002-2.

Kopeikina, K. J., Carlson, G. A., Pitstick, R., Ludvigson, A. E., Peters, A., Luebke, J. I., Koffie, R. M., Frosch, M. P., Hyman, B. T., & Spires-Jones, T. L. (2011). Tau accumulation causes mitochondrial distribution deficits in neurons in a mouse model of Tauopathy and in Human alzheimer's disease brain. *The American Journal of Pathology*, 179(4), 2071–2082. https://doi.org/10.1016/j.ajpath.2011.07.004

Kraeuter, A.-K., Guest, P. C., & Sarnyai, Z. (2019). The Elevated Plus Maze for Measuring Anxiety-Like Behavior in Rodents. *Methods in Molecular Biology*, 1916, 69-74. doi: 10.1007/978-1-4939-8994-2_4

Lane, C. A., Hardy, J., & Schott, J. M. (2017). Alzheimer's disease. European Journal of *Neurology*, 25(1), 59–70. https://doi.org/10.1111/ene.13439

Liu, M.-Y., Yin, C.-Y., Zhu, L.-J., Zhu, X.-H., Xu, C., Luo, C.-X., Chen, H., Zhu, D.-Y., & Zhou, Q.-G. (2018). Sucrose preference test for measurement of stress-induced anhedonia in mice. *Nature Protocols*, 13(7), 1686-1698. doi: 10.1038/s41596-018-0011-z

López-Arrieta, J. M., & Birks, J. (2002). Nimodipine for primary degenerative, mixed and vascular dementia. *The Cochrane Database of Systematic Reviews*, 3, CD000147. López-Cuenca, I. (2022). The relationship between retinal layers and brain areas in asymptomatic first-degree relatives of sporadic forms of Alzheimer's disease: An exploratory analysis. *Alzheimer's Research & Therapy*, *14*(1), 1–18. https://doi.org/10.1186/s13195-022-01008-5

Mandelkow, E.-M., Biernat, J., Drewes, G., Gustke, N., Trinczek, B., & Mandelkow, E. (1995). Tau domains, phosphorylation, and interactions with microtubules. *Neurobiology of Aging*, 16(3), 355–362. https://doi.org/10.1016/0197-4580(95)00025-a

Marzetti, E., & Leeuwenburgh, C. (2006). Skeletal muscle apoptosis, sarcopenia and frailty at old age. *Experimental Gerontology*, 41(12), 1234–1238. https://doi.org/10.1016/j.exger.2006.08.011

Moreira, P. I., Carvalho, C., Zhu, X., Smith, M. A., & Perry, G. (2010). Mitochondrial dysfunction is a trigger of alzheimer's disease pathophysiology. *Biochimica et Biophysica Acta (BBA) - Molecular Basis of Disease,* 1802(1), 2–10. https://doi.org/10.1016/j.bbadis.2009.10.006

Moore, S. J., & Murphy, G. G. (2020). The role of L-type calcium channels in neuronal excitability and aging. *Neurobiology of Learning and Memory*, 173, 107230. https://doi.org/10.1016/j.nlm.2020.107230

Nahirney, P. C., & Tremblay, M.-E. (2021). Brain ultrastructure: Putting the pieces together. *Frontiers in Cell and Developmental Biology*, *9*. https://doi.org/10.3389/fcell.2021.629503

Omoluabi, T., Torraville, S. E., Maziar, A., Ghosh, A., Power, K. D., Reinhardt, C., Harley, C. W., & Yuan, Q. (2021). Novelty-like activation of locus coeruleus protects against deleterious human pre-effects. *Alzheimer's and Dementia*, *7*(1), e1223. https://doi.org/10.1002/trc2.12231

Osellame, L. D., Blacker, T. S., & Duchen, M. R. (2012). Cellular and molecular mechanisms of mitochondrial function. *Best Practice & Research Clinical Endocrinology & Metabolism*, 26(6), 711–723. https://doi.org/10.1016/j.beem.2012.05.003

Palmer, C. S., Osellame, L. D., Stojanovski, D., & Ryan, M. T. (2011). The regulation of mitochondrial morphology: Intricate mechanisms and dynamic machinery. *Cellular Signalling*, 23(10), 1534–1545. https://doi.org/10.1016/j.cellsig.2011.05.021

Patel, R. S., Rachamalla, M., Chary, N. R., Shera, F. Y., Tikoo, K., & Jena, G. (2012). Cytarabine induced cerebellar neuronal damage in juvenile rat: Correlating neurobehavioral performance with cellular and genetic alterations. *Toxicology*, 293(1–3), 41–52. https://doi.org/10.1016/j.tox.2011.12.005

Paxinos, G., & Watson, C. (2014). Paxinos and Watson's The Rat Brain in stereotaxic coordinates. Academic Press.

Pickett, E. K., Rose, J., McCrory, C., McKenzie, C.-A., King, D., Smith, C., Gillingwater, T. H., Henstridge, C. M., & Spires-Jones, T. L. (2018). Region-specific depletion of synaptic mitochondria in the brains of patients with alzheimer's disease. *Acta Neuropathologica*, 136(5), 747–757. https://doi.org/10.1007/s00401-018-1903-2

Poe, G. R., Foote, S., Eschenko, O., Johansen, J. P., Bouret, S., Aston-Jones, G., Harley, C. W., Manahan-Vaughan, D., Weinshenker, D., Valentino, R., Berridge, C., Chandler, D. J., Waterhouse, B., & Sara, S. J. (2020). Locus coeruleus: A new look at the blue spot. *Nature Reviews. Neuroscience*, *21*(11), 644–59. https://doi.org/10.1038/s41583-020- 0360-9

Redpath, C.J., Khalil, M.B., Drozdzal, G., Radisic, M., McBride, H.M. (2013). Mitochondrial hyperfusion during oxidative stress is coupled to a dysregulation in calcium

handling within a C2C12 cell model. *PLoS One*, 8 (7), https://doi.org/10.1371/journal.pone.0069165.

Rizzuto, R., De Stefani, D., Raffaello, A., & Mammucari, C. (2012). Mitochondria as sensors and regulators of calcium signalling. *Nature Reviews Molecular Cell Biology*, 13(9), 566–578. https://doi.org/10.1038/nrm3412

Ryan, K. C., Ashkavand, Z., & Norman, K. R. (2020). The role of mitochondrial calcium homeostasis in Alzheimer's and related diseases. *International Journal of Molecular Sciences*, *21*(23), 9153. PMCID: PMC7730848

Serrano-Pozo, A., Frosch, M. P., Masliah, E., & Hyman, B. T. (2011). Neuropathological alterations in Alzheimer disease. *Cold Spring Harbor Perspectives in Medicine*, 1(1). https://doi.org/10.1101/cshperspect.a006189

Schneider, C. A., Rasband, W. S., Eliceiri, K. W. (2012). NIH image to ImageJ: 25 years of image analysis. *Nature Methods,* 9, 671–75. https://www.nature.com/articles/nmeth.2089

Seibenhener, M. L. & Wooten, M. C. (2015). Use of the open field maze to measure locomotor and anxiety-like behavior in mice. *Journal of Visualized Experiments, 96*, e52434. doi: 10.3791/52434

Sesso, A., Belizário, J. E., Marques, M. M., Higuchi, M. L., Schumacher, R. I., Colquhoun, A., Ito, E., & Kawakami, J. (2012). Mitochondrial swelling and incipient outer membrane rupture in preapoptotic and apoptotic cells. *The Anatomical Record*, 295(10), 1647–1659. https://doi.org/10.1002/ar.22553

Shahpasand, K., Uemura, I., Saito, T., Asano, T., Hata, K., Shibata, K., Toyoshima, Y., Hasegawa, M., & Hisanaga, S. (2012). Regulation of mitochondrial transport and inter-microtubule spacing by tau phosphorylation at the sites hyperphosphorylated in Alzheimer’s

disease. *The Journal of Neuroscience*, 32(7), 2430–2441. https://doi.org/10.1523/jneurosci.5927-11.2012

Shankar, G. M., Li, S., Mehta, T. H., Garcia-Munoz, A., Shepardson, N. E., Smith, I., Brett, F. M., Farrell, M. A., Rowan, M. J., Lemere, C. A., Regan, C. M., Walsh, D. M., Sabatini, B. L., & Selkoe, D. J. (2008). Amyloid-β protein dimers isolated directly from Alzheimer's brains impair synaptic plasticity and memory. *Nature Medicine,* 14(8), 837–842. https://doi.org/10.1038/nm1782

Shults, N.V., Kanovka, S.S., Ten Eyck, J.E., Rybka, V., Suzuki, Y.J. (2019). Ultrastructural changes of the right ventricular myocytes in pulmonary arterial hypertension. *Am. Heart J*. 8 (5), e011227. https://doi.org/10.1161/JAHA.118.011227.

Sundermann, E. E., Panizzon, M. S., Chen, X., Andrews, M., Galasko, D., & Banks, S. J. (2020). Sex differences in alzheimer's-related tau biomarkers and a mediating effect of testosterone. *Biology of Sex Differences,* 11(1). https://doi.org/10.1186/s13293-020-00310-x

Susin, S. A., Lorenzo, H. K., Zamzami, N., Marzo, I., Snow, B. E., Brothers, G. M., Mangion, J., Jacotot, E., Costantini, P., Loeffler, M., Larochette, N., Goodlett, D. R., Aebersold, R., Siderovski, D. P., Penninger, J. M., & Kroemer, G. (1999). Molecular characterization of mitochondrial apoptosis-inducing factor. *Nature*, 397(6718), 441–446. https://doi.org/10.1038/17135

Swerdlow, R. H., & Khan, S. M. (2009). The alzheimer's disease mitochondrial cascade hypothesis: An update. *Experimental Neurology*, 218(2), 308–315. https://doi.org/10.1016/j.expneurol.2009.01.011

Szabo, L., Eckert, A., & Grimm, A. (2020). Insights into disease-associated tau impact on mitochondria. *International Journal of Molecular Sciences*, *21*(17), 6344. https://doi.org/10.3390/ijms21176344

Terman, A., Kurz, T., Navratil, M., Arriaga, E.A., Brunk, U.T. (2010). Mitochondrial turnover and aging of long-lived postmitotic cells: the mitochondrial–lysosomal axis theory of aging. *Antioxid. Redox Signal.* 12 (4), 503–535. https://doi.org/10.1089/ ars.2009.2598.

Tsuboi, Y., Josephs, K. A., Boeve, B. F., Litvan, I., Caselli, R. J., Caviness, J. N., Uitti, R. J., Bott, A. D., & Dickson, D. W. (2005). Increased tau burden in the cortices of progressive supranuclear palsy presenting with corticobasal syndrome. *Movement Disorders*, 20(8), 982–988. https://doi.org/10.1002/mds.20478

Vassar, R., Bennet, B. D., Babu-Khan, S., Kahn, S., Mendiaz, E. A., Denis, P., Teplow, D. B., Ross, S., Amarante, P., Loeloff, R., Luo, Y., Fisher, S., Fuller, J., Edenson, S., Lile, J., Jarosinski, M. A., Biere, A. L., Curran, E., Burgess, T., Citron, M. (1999). Secretase 57 cleavage of Alzheimer's amyloid precursor protein by the transmembrane aspartic protease BACE. *Science*, 286, 735-741. doi: 10.1126/science.286.5440.735

Vossel, K. A., Zhang, K., Brodbeck, J., Daub, A. C., Sharma, P., Finkbeiner, S., Cui, B., & Mucke, L. (2010). Tau reduction prevents AB-induced defects in axonal transport. *Science*, 330(6001), 198–198. https://doi.org/10.1126/science.1194653

Walker, B. R., & Moraes, C. T. (2022). Nuclear-mitochondrial interactions. *Biomolecules,* 12(3), 427. https://doi.org/10.3390/biom12030427

Weingarten, M. D., Lockwood, A. H., Hwo, S. Y., & Kirschner, M. W. (1975). A protein factor essential for microtubule assembly. *Proceedings of the National Academy of Sciences,* 72(5), 1858–1862. https://doi.org/10.1073/pnas.72.5.1858

Weinshenker, D. (2008). Functional consequences of locus coeruleus degeneration in Alzheimer's disease. *Current Alzheimer Research*, 5(3), 342–345. https://doi.org/10.2174/156720508784533286

Wilson, R. S., Nag, S., Boyle, P. A., Hizel, L. P., Yu, L., Buchman, A. S., Schneider, J. A., & Bennet, D. A. (2013). Neural reserve, neuronal density in the locus coeruleus, and cognitive decline. *Neurology*, 80(13), 1202-1208. doi: 10.1212/WNL.0b013e3182897103

Yang, Y., & Schmitt, H. P. (2001). Frontotemporal Dementia: Evidence for impairment of ascending serotoninergic but not noradrenergic innervation. Acta Neuropathologica, 101(3), 256–270. https://doi.org/10.1007/s004010000293

Appendices

I Perfusion Chemicals and Buffer Solutions

Chemicals and buffers used for transcardial rat perfusions per the Geinisman protocol.

Chemicals:

1. Sodium phosphate dibasic (anhydrous)
2. Sodium phosphate monobasic
3. Heparin sodium salt
4. Glutaraldehyde solution
5. Calcium chloride
6. Paraformaldehyde
7. Sodium hydroxide
8. Hydrochloric acid

Buffers:

- 0.2M Phosphate buffer saline
  a. Na_2PO_4 dibasic (50g of crystals in 1750ml DH_20)
  b. Na_2PO_4 monobasic (14g of crystals in 500ml DH_20)

  0.1M Sorenson's buffer (3600ml)
  a. Na_2PO_4 dibasic (1392ml)
  b. Na_2PO_4 monobasic (408ml)
  c. DH_2O (1800ml)
  d. pH of 7.3 to 7.4 (correct pH with either HCl or NaOH)

- Fix
  a. Full-strength solution (2% paraformaldehyde; 2.5% glutaraldehyde)
  For 3500ml of fix (full strength fix):

i. Combine 70g of paraformaldehyde with 3255 ml of Sorensen's buffer (Do not heat past 45 ^{0}C). Dissolve paraformaldehyde with NaOH.
ii. Filter the solution
iii. Add 175ml of 50% glutaraldehyde
iv. pH of 7.3 to 7.4
v. Add 10mg of $CaCl_2$

b. Half-strength solution (1% paraformaldehyde; 1.25% glutaraldehyde)

- Prewash solution
  a. 125mg of heparin in either 500ml 0.2M phosphate buffer saline or 0.1M Sorenson's buffer
  b. 30ml per rat

II Vibratome Procedure

25ml borosilicate glass vials with black phenolic caps were used to store the perfused tyrosine hydroxylase (TH)-CRE rat brains. The brains were fully submerged in vials filled with 0.1M Sorensen's phosphate buffer solution. Brains were kept in the refrigerator at 4°C when not in use.

To prepare brains for the vibratome, a coronal cross-section was cut anterior to the pineal gland and posterior to the hippocampus. The anterior brain half, which contains the hippocampus, was stored for the completion of another project. The posterior brain half had a supplementary coronal cross-section located posterior to the cerebellum to provide a flattened surface. The flattened posterior of the posterior brain half was glued to the base of the vibratome boat to ensure the anterior portion was facing upwards. Once the glue was completely dry, 0.1M Sorensen's phosphate buffer solution was pipetted over the brain to prevent the tissue from drying out as well as shrinkage. The boat was then locked into the Pelco 102 Vibratome Sectioning System. Using injector carbon steel blades, sections of 700µm thickness were sliced.

The Rat Brain in Stereotaxic Coordinates 6th edition by George Paxinos and Charles Watson was used to graphically assess the location and depth of slices according to bregma (- 9.48 to -10.44). The LC is located bilaterally, ventral to the outermost curve of the fourth ventricle. Serial sections were cut until the fourth ventricle walls separated, forming a visible lumen, which indicated the entire LC structure was in the previous slices.

Soft bristle brushes and forceps were used to gently move the slices in the boat. The slices were lifted by slowly scooping underneath to rest slices across the top face of the brush. While removing the slices from the vibratome boat, the brush was flipped to invert the brain slices so that the anatomical right was facing the right-hand side. Slices were placed in order from anterior to posterior onto labelled filter paper.

Slices had 0.1M Sorensen's phosphate buffer pipetted over the faces to ensure the tissue remained moist. Extra slices to reach the LC were disposed of in proper waste containers. This procedure was repeated for 25 brains.

III Locus Coeruleus Dissections

Approximately 3-4 slices of tissues containing the LC were selected and brought to the Olympus SZ61 dissecting microscope. Using a scalpel, the LC was dissected out into a small square. A notch was cut out in the corner pointing towards LC as a means to identify the orientation of the square in the tissue block. Squares included the outmost curve of the 4th ventricle to help identify the location of the LC. LC tissue squares were placed into 4ml borosilicate glass vials with phenolic screw caps. Labelled vials were filled with 0.1M Sorensen's phosphate buffer solution and stored at 4°C until the embedding procedure.

IV Locus Coeruleus Tissue Embedding

A solution of 2% osmium tetroxide was created by diluting 4% osmium tetroxide with 0.1M Sorensen's phosphate buffer solution. Each LC-containing vial had the buffer solution removed and then replaced with the 2% osmium solution. This was pipetted into each vial until the tissue blocks were completely covered. Vials were placed into plastic holding trays to keep them upright. For 1 hour, the vials sat on the platform shaker for solute particles to be evenly distributed throughout the solution and to ensure the tissue was stained homogeneously.

After 1 hour, the osmium solution was removed from the vials and the vials were re-filled with 50% ethanol alcohol (EtOH). The vials sat for 15 minutes on the platform shaker to begin slowly dehydrating the tissue. The empty-refill procedure for this dehydrating process was repeated with 70% EtOH for 15 minutes on the platform shaker, followed by 90% EtOH for 10 minutes, and lastly 100% EtOH for 10 minutes.

A solution of half EtOH and half LR white resin was created. LR white resin is a hydrophilic acrylic resin of low viscosity with wide applications suitable for both light and electron microscopy. The LR white resin bottles were stored at 4°C until use. Once the 100% ethanol was removed, the 1:1 EtOH and resin were pipetted into each vial and placed on the platform shaker for 30-minute intervals to slowly begin infiltrating the resin into the tissue. The solution was removed and replaced with fresh solutions 5 times.

The final 1:1 solution was removed and replaced with 100% LR white resin. Vials were placed on the platform shaker for 2 hours. After two hours, the 100% LR white resin was removed and replaced with new 100% LR white resin. Vials were placed on the platform shaker for 1 more hour.

Gelatin capsules with a volume of 0.95ml and 8.18mm diameter were placed into plastic capsule trays. Each capsule had a paper identification code placed inside along the rim of the capsule to identify each tissue block. Approximately, 2-3 drops of 100% LR white resin were dropped at the bottom of each capsule. The tissue blocks were removed from the glass vials and maneuvered using bamboo skewers, then carefully placed at the bottom of the gelatin capsules, ensuring the wide surface of the tissue was directly in the center at the bottom of the capsule. The gelatin capsules were filled until the resin touched the top rim of the gelatin capsule, allowing room for the resin to set without leaking. The lids were placed back onto the capsules.

During the embedding procedure, the Isotemp 500 Series Laboratory Oven was preheated to 55°C. The filled capsules were brought to the oven and placed on the middle rack. For polymerization of the resin to occur, the resin was heat-cured for 48 hours. For the first 24 hours, the oven was set at 55°C, then the temperature was increased to 60°C for the remaining 24 hours.

V Gelatin Capsule Removal

A 4L glass beaker filled with water was heated on a hotplate to 75°C. The cured gelatin capsules were placed into the 75°C water. Using a magnetic stir bar, a vortex was created to keep water movement and prevent heat damage to the resin blocks. The capsules remained in the water until the gelatin melted off the resin, which took approximately 30 minutes. Once the gelatin was melted or softened, the capsules were removed from the water. Using a paper towel, excess gelatin was removed. Clean and dried resin blocks were stored in their corresponding storage boxes.

VI Initial Resin Block Trim

Resin blocks were locked into an aluminum chuck with roughly two-thirds of the resin block exposed and the tissue block facing outwards. The chuck was locked into the Leica EM Trim. The overburden of resin was shaved off at 0° to create a flat surface, the initial overburden resin was shaved until the tissue became exposed from the resin. If the tissue settled incorrectly and was embedded at an angle, the angle used to create a flat face was recorded to assist with setting the ultracut parameters. The chuck was titled between a 30°- 40° angle and the sides of the resin were ground down until the exposed tissue was trimmed to a trapezoid. Trapezoid orientation was acquired based on positioning the 4^{th} ventricle proximal to the short parallel face of the trapezoid. Peripheral resin was reserved surrounding the sides of the trapezoids to prevent losing tissue in the initial trims.

VII Thick Cut Procedure

The glass knives were locked into the Leica Ultracut R and the basin was filled with distilled water. Parameters were set to cut 1000nm slices. Distilled water was pipetted onto a labelled glass microscope slide. Tweezers were used to gently scoop the tissue slices from the surface of the water basin and to lay slices on top of the water drops on the glass slide.

Glass slides were placed onto a hotplate set to heat level 3 to allow evaporation and to fix the tissue to the slide, carefully ensuring the tissue did not burn. Once completely dried, toluidine blue O stain was pipette over the tissue until completely covered. The glass slide remained on the hot plate until a silver rim formed around the stain drop, which was approximately 1 minute. The stain was rinsed off with a squirt bottle filled with distilled water. The remaining water was removed by resting the slide on the hotplate until dry. Glass sides were stored in slide boxes.

VIII Glass Knife Procedure

Glass bars with dimensions of 25mm, 6.5mm, by 400mm were cut using the Leica EMKMR glass cutter. The bars were continuously cut into halves until equilateral squares were formed. Squares were cut at a 45° angle to create 2 triangles. The silver tape was wrapped around the sharp edge of the triangle on the hypotenuse side perpendicular to the base which created a basin behind the blade. A clear liquid adhesive was painted around the edge of the tape to create a watertight seal. Knives were set aside to ensure the adhesive was completely dry before use.

IX Toluidine Blue O Shipped

A measurement of 10g sodium borate was added to 500 ml of warm distilled water. A metal stir bar created a vortex to mix the solution. The solution was stirred until a transparent appearance was achieved. A weight of 5g of Toluidine Blue O was added and mixed for 20 minutes until no precipitate was visible. The stain was strained through filter paper to remove any remaining precipitate.

X Thin Cutting Procedure

Silver to pale blonde-coloured slices were obtained by setting the parameters of the Leica Ultracut R to cut at 60-65nm thick on the DiATOME 45° diamond knife. The blade of the diamond knife was first cleaned with a Styrofoam bar. Once locked into the ultracut, the basin of the diamond knife was filled with distilled water. The resin block was positioned so that the wide

parallel edge of the trapezoid was on the bottom. Slices were cut to form a ribbon of tissue across the top of the water basin. A ribbon of 20 slices was the goal. If a dark gold slice was seen in the ribbon, it was removed and recorded. A cotton swab dipped in chloroform was gently hovered over the tissue surface to gently spread the tissue and help prevent folding. The ribbon was broken into smaller ribbons of 4-5 slices. Approximately 3 copper 300-line square mesh grids (depending on the confidence that tissue properly adhered to the grids) were tapped onto tissue ribbons of 4-5 slices so that the tissue stuck to the dull side of the copper grids. Copper grids were laid tissue side up onto a grid-grid to air dry. Once dried, copper grids were stored in their corresponding slots in the grid boxes.

XI Ethics Approval Documentation

MEMORIAL UNIVERSITY

Dear: Dr. Qi Yuan, Faculty of Medicine\Division of BioMedical Sciences

Researcher Portal File No.: 20220211
Animal Care File:
Entitled: Locus coeruleus norepinephrine modulation in learning and Alzheimer's Disease
Status: Active
Related Awards:

Awards File No	Title	Status	
20190269	Material Transfer Agreement - Not Publishable	Active	1. Research Grant and Contract Services (RGCS) – St. John's and Grenfell Campuses
20191784	Locus coeruleus NE modulation in learning and Alzheimer's disease	Active	1. Research Grant and Contract Services (RGCS) – St. John's and Grenfell Campuses
20200652	MTA for cis p-tau antibody from Harvard University	Active	1. Research Grant and Contract Services (RGCS) – St. John's and Grenfell Campuses
20200817	Understanding what pretangle tau does to neurons and testing potential damage control by an anti-cis-ptau treatment	Active	1. Research Grant and Contract Services (RGCS) – St. John's and Grenfell Campuses

Ethics Clearance Terminated: May 01, 2024

Your three-year renewal application was reviewed by the ACC on Tuesday June 1, 2021, and the committee approved the renewal, however they did note to please write lay summaries in simpler terms in the future.

This ethics clearance includes the following Team Members: Dr. Qi Yuan (Principal Investigator)
Dr. Xihua Chen (Co-Investigator)
Dr. Susan Walling (Co-Investigator)
Dr. Carolyn Harley (Co-Investigator)

This ethics clearance includes the following Sponsors: [[AllSponsorAgencyNames]]
This ethics clearance includes the following related awards:

Awards File No	Title	Status	
20190269	Material Transfer Agreement - Not Publishable	Active	1. Research Grant and Contract Services (RGCS) – St. John's and Grenfell Campuses
20191784	Locus coeruleus NE modulation in learning and Alzheimer's disease	Active	1. Research Grant and Contract Services (RGCS) – St. John's and Grenfell Campuses
20200652	MTA for cis p-tau antibody from Harvard University	Active	1. Research Grant and Contract Services (RGCS) – St. John's and Grenfell Campuses
20200817	Understanding what pretangle tau does to neurons and testing potential damage control by an anti-cis-ptau treatment	Active	1. Research Grant and Contract Services (RGCS) – St. John's and Grenfell Campuses

An Event [Annual Report] will be required following each year of protocol activity.

Should you encounter an unexpected incident that negatively affects animal welfare or the research project relating to animal use, please submit an Event [Incident Report].

Any alterations to the protocol requires prior submission and approval of an Event [Amendment].

NOTE: You can access a copy of this email at any time under the "Shared Communications" section of the Logs tab of your file in the Memorial Researcher Portal.

Sincerely,

ANULIKA MBAKWE | ACC COORDINATOR
Department of Animal Care Services
Memorial University of Newfoundland
Health Sciences Centre | Room H1848
P: 709-777-6621
E-Mail: ambakwe@mun.ca